Geoffrey LEZIER

Nanotech Master

2020

CEA-Spintec

Study of RF-to-DC conversion using spintronic devices

from 02/03/2020 to 17/07/2020

Under the supervision of :

- **Spintec supervisor : Ursula EBELS, ursula.ebels@cea.fr**
- **Phelma Tutor : Liliana PREJBEANU, liliana.buda@cea.fr**

Ecole nationale
Supérieure de physique,
Électronique, Matériaux

Phelma
Bât. Grenoble INP - Minatec
3 Parvis Louis Néel - CS 50257
F-38016 Grenoble Cedex 01

Tél +33 (0)4 56 52 91 00
Fax +33 (0)4 56 52 91 03

http://phelma.grenoble-inp.fr

Outline

Acknowledgement

This internship was realized during a very exceptional time, and despite this situation, I really enjoyed my time working at Spintec.

I would like to thank Sylvain, Artem, Mario and Mateo, for the time I've spent with them (in person or via skype) and for the help they provided during this project.

I want to make special thanks to Ahmed, who facilitated my integration in the team, on the project and provided very helpful insights and interpretations on my results.

Thank you to Liliana, who helped me through the project, and that kept tabs on me to check how the internship was progressing, and how things were generally going.

Finally, I am grateful that I was able to work with Ursula, who was a great mentor to me during these hard times, and that showed patience and great pedagogic skills, despite the uneasy situation happening at the time.

And a special thanks to all the people I have interacted with at Spintec, all the PhDs, the Postdocs and the permanent people that I talked to, and that made my experience at Spintec better.

Glossary

ANR : Agence Nationale de la Recherche
MTJ : Magnetic Tunnel Junction
RF : Radio-Frequency
DC : Direct Current
FL : Free Layer
PL : Polarizing Layer
MRAM: Magnetic Random-Access Memory
MR: MagnetoResistance
STT: Spin Transfer Torque
GMR: Giant MagnetoResistance
TMR: Tunneling MagnetoResistance
FM: FerroMagnetic
BCC: Body-Centered Cubic
SAF: Synthetic AntiFerromagnet
FMR: FerroMagnetic Resonance
LLG: Landau-Lifshitz-Gilbert
WuRX: Wake-up Receiver
RxDemod: Reception Demodulation
WPH: Wireless Power Harvester
MRH: MagnetoResistance Hysteresis
Happ: Applied magnetic field
PSD: Power Spectral Density
HIP: In-plane magnetic field
HOP: Out-of-plane magnetic field

I. Introduction

A. Objectives of the project

The purpose of this project is to understand and characterize the oscillating properties of Magnetic Tunnel Junction in order to realize an RF-to-DC conversion of an electrical signal.
This project was carried out in the frame of the research project "SPINNET" funded by the ANR. SPINNET focuses on the RF-to-DC conversion function to explore possible applications for Wireless Sensor Networks.

My role was to study MTJs devices that have been realized within a former project "GREAT" (funded by the EC within the Horizon2020 framework), whose purpose was to explore the possibility to use the same MTJ stacks for four different functions: memory, logic, sensing and RF applications. For these devices, I characterized their RF-to-DC conversion properties as a function of the device geometries (size and diameter) but also with the externally applied perturbations (magnetic field, DC current).

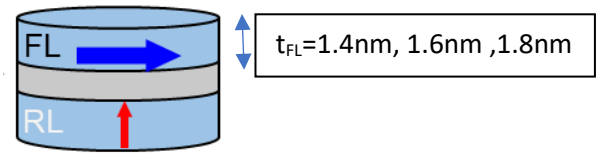

Figure 1: Simplified schematics of the device

A set of three devices varying in FL thickness were available, see Figure 1. The 1.4nm and 1.8nm devices have been previously characterized by other team members, and I concentrated on the 1.6nm devices. The preliminary experiments showed good, if not best conversion efficiencies.

After an introduction on the basics of spintronics, I will describe the experimental setup, and then proceed with the results and analysis of the experiments.

B. Presentation of the lab

Spintec is a research laboratory at the crossroad of fundamental and applied research in the field spintronics. Considered as one of the leaders in this field, Spintec has developed a wide range of concepts, technologies, and has even spun-off start-ups such as Crocus technologies, that is now recognized for their expertise in spintronics and MRAM technologies.
The lab is divided in multiple research teams that each focus on different aspects of magnetism and spintronics : from Theory&Simulations to Sensors and Health&Biology groups, the ~100 people working in the lab cover almost all aspects of research in magnetism and spintronics [1].

II. Basics of spintronics

To understand the RF-to-DC conversion properties, a set of basic notions in spintronics are necessary. In this part, some spintronics phenomena will be summarized such as MagnetoResistance, Spin Transfer Torque, and magnetization dynamics.

A. Magnetic Tunnel Junction

1. GMR/TMR

The Giant Magnetoresistance, or GMR, is one of the founding principles of spintronics, and has been a subject of studies for scientists for nearly three decades, following its discovery in 1988. The GMR is based on the difference of resistivity of a multi-layer device, two ferromagnetic layers separated by a non-magnetic layer whose magnetization are either parallel or antiparallel.

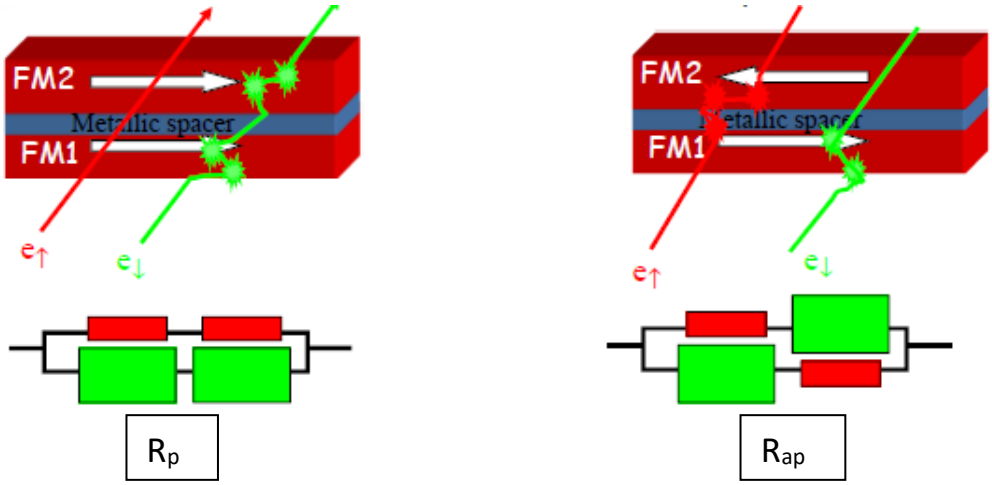

Figure 2: Simplified schematics of GMR phenomena; on the left, the parallel configuration, and on the right, the antiparallel configuration

$$Rp = 2\frac{\rho\uparrow.\rho\downarrow}{\rho\uparrow+\rho\downarrow} < Rap = \frac{\rho\uparrow+\rho\downarrow}{2}$$

This physical principle is the one used in the MRAM technologies, since two stable states of the system are possible: parallel or antiparallel, “0 “or “1”, as shown in figure 2 [2].

The Tunneling Magnetoresistance, or TMR, is based upon the spin dependent tunneling of electron through a crystalline oxide barrier, detailed in figure 3.

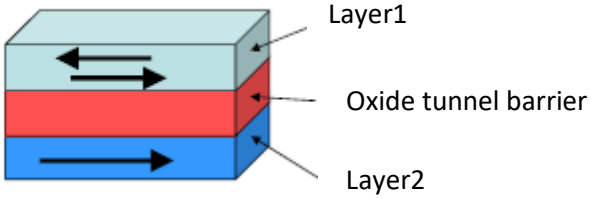

Figure 3 : Classic magnetic system with 2 ferromagnetics and a non-magnetic spacer

The Julliere’s model describes the phenomena using the spin polarization of each layer; the TMR ratio is defined by:

$$TMR = 2\frac{P1.P2}{1-P1.P2}$$

Where P1, P2 are the spin polarization of the layer 1 and 2 respectively.
The TMR high ratio is due to the very selective spin filtering of a crystalline oxide barrier:

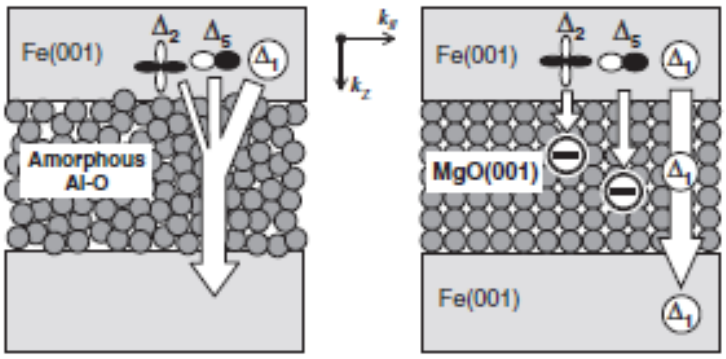

Figure 4: Spin coherent tunneling in amorphous and crystalline oxide

The coherent spin-dependent tunneling in an epitaxial MTJ allows for a specific spin state to cross the barrier, as explained in figure 4.
This principle allows for a much higher MR ratio than GMR, with values going up to several hundred percent at extremely low temperature [3].

2. Description of the junction

The junctions used in this project correspond to a classic Metallic Tunnel Junction (MTJ), usually used for memory purposes.
The MTJ is composed of 4 magnetic layers, each one with a specific role in the perpendicular configuration (the magnetization is perpendicular with respect to the horizontal plane).

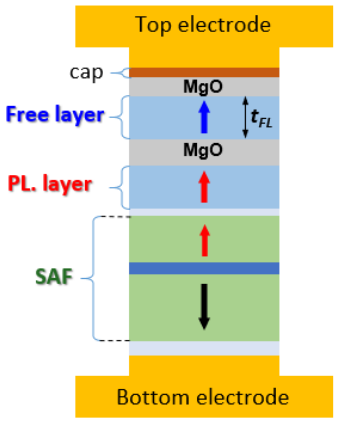

MgO (2x140) / (0.4 nm) **Pt** / (3 nm) **Ta** / (7 nm) **Ru** /
(**t nm**) **$Co_{20}Fe_{60}B_{20}$**/ (0.3 nm) **W** / (0.5 nm) **$Co_{20}Fe_{60}B_{20}$**/
MgO (2x125)/
(0.9 nm) **Co** / (0.25 nm) **W** / (1 nm) **$Co_{17}Fe_{53}B_{30}$**/
(0.2 nm) **Pt** / (0.15 nm) **Ta** /
(0.6 nm) **Co** / **3x**[(0.2 nm) **Pt** / (0.5 nm) **Co**] /
(0.8 nm) **Ru** /
(1.5 nm) **Pt** / **6x**[(0.5 nm) **Co** / (0.2 nm) **Pt**] / (0.6 nm) **Co** /
Etch / (0.7 nm) **Ta** /

Figure 5 : Configuration of the MTJ

The Polarizing Layer and the Free Layer are the two active parts used for the storage of information when this structure is used as a memory cell.
These two layers are separated by an oxide layer, in this case MgO. This oxide has different purposes; it creates a perpendicular interfacial anisotropy that forces these layers to be in a perpendicular configuration, but it is also necessary to produce a large TMR and spin selectivity. The MgO layer is deposited as an amorphous thin film and crystallizes upon. The polarizing and free layers are made of CoFeB, deposited as an amorphous thin film. Upon annealing, the already textured MgO sees its BCC crystallinity improve and forces a BCC (body-centered cubic) crystallization of the free and polarizing

layers, ejecting in the meantime the Boron atoms out of the CoFe alloy. The external layers (Ta & Ru) [4] act as a Boron pump. It is important to 'pump' the Boron atoms away from the oxide to prevent the formation of BO complexes that reduces interfacial anisotropy and TMR properties, but also impacts the barrier endurance.
The two « memory » layers and the intermediate MgO must have a BCC crystalline configuration to maximize TMR. The composition of the magnetic layer has been chosen to maximize the tunneling capabilities of the junction, both in terms of amplitude and selectivity of the spin currents.

The third and fourth part of the MTJ corresponds to the SAF (Synthetic AntiFerromagnet) layers.
The SAF is not supposed to play a role in the « memory » part of the MTJ, but rather has a role of stabilizing and enhancing the properties of the free and polarizing layers. With a strong perpendicular anisotropy, these layers reduce the magnetostatics stray field of the free layer.
The strong magnetic anisotropy comes from the alternating Pt and Co layers that compose the SAF, and the antiferromagnetic coupling comes from the intermediate Ru layer.

B. Magnetization dynamics

In order to comprehend the physical principles of detection, an analysis of the static and dynamic state of the magnetization in the different layers allows us to predict the potential conversion of the signal.

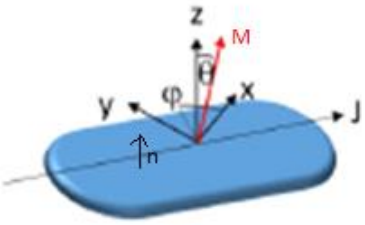

Figure 6: Schematics of a magnetic layer

1. Energy and effective field

a) Equilibrium positions

Since the field that we are using in our experiments are in Oersted, the following equations are written in the cgs unit system and describe the figure 6.
We define the energy in the layer as:

$$E = K\left(1 - (\boldsymbol{nm})^2\right) - (\boldsymbol{MH_a}) + 2\pi\boldsymbol{M}\left(\bar{\bar{\boldsymbol{N}}}\boldsymbol{M}\right)$$

With:

$$\bar{\bar{\boldsymbol{N}}} = \begin{pmatrix} 0 & 0 & 0 \\ 0 & 0 & 0 \\ 0 & 0 & 1 \end{pmatrix}; \quad \boldsymbol{n} = \begin{pmatrix} 0 \\ 0 \\ 1 \end{pmatrix}; \quad \boldsymbol{H_a} = H_a \begin{pmatrix} cos\varphi_H \\ sin\varphi_H \\ 0 \end{pmatrix} = \begin{pmatrix} H_a \\ 0 \\ 0 \end{pmatrix} \text{ the applied field;}$$

$$\boldsymbol{m} = \begin{pmatrix} sin\theta cos\varphi \\ sin\theta sin\varphi \\ cos\theta \end{pmatrix}$$

$H_u = \frac{2K_i}{M_s t}$ the anisotropy field; $H_d = 4\pi M_s$ the demagnetizing field ; K_i the interface anisotropy

We define $Q = \frac{H_u}{H_d}$, the ratio between the anisotropy field and the demagnetizing field.
Q defines the relative contribution of the in-plane field (Hd) and the out-of-plane field (Hu) that dictates whether the magnetization of the layer is in-plane or out-of-plane.

We define the energy derivatives:

$$E_\varphi = \frac{\partial E}{\partial \varphi} = M_s\, H_a \sin\theta \sin\varphi$$

$$E_{\varphi\varphi} = \frac{\partial^2 E}{\partial \varphi^2} = M_s\, H_a \sin\theta \cos\varphi$$

$$E_{\theta\varphi} = \frac{\partial^2 E}{\partial \theta\, \partial \varphi} = \frac{\partial^2 E}{\partial \varphi\, \partial \theta} = M_s\, H_a \cos\theta \sin\varphi$$

$$E_\theta = \frac{\partial E}{\partial \theta} = -\frac{M_s}{2}(H_d - H_u)2\sin\theta\cos\theta - M_s\, H_a \cos\theta\cos\varphi$$

$$E_{\theta\theta} = \frac{\partial^2 E}{\partial \theta^2} = -\frac{M_s}{2}(H_d - H_u)2\cos 2\theta + M_s\, H_a \sin\theta\cos\varphi$$

For example, an in-plane stable point ($\varphi = 0°$) would be:

$$E_\varphi = 0 \; for \; \varphi = 0°$$

$$E_\theta = 0 \rightarrow (\varphi = 0°): -M_s \cos\theta(H_a + (H_d - H_u)\sin\theta) = 0 \;\rightarrow \theta = 90° \text{ or } \sin\theta = \frac{-H_a}{(H_d - H_u)}$$

Stability:

$$E_{\theta\theta} = \frac{\partial^2 E}{\partial \theta^2} = -\frac{M_s}{2}(H_d - H_u)2\cos 2\theta + M_s\, H_a \sin\theta$$

Case 1:

For $\theta = 90° \rightarrow E_{\theta\theta} = Ms(Hd - Hu) + MsHa = Ms(Hd(1 - Q) + Ha)$

If Q<1, $E_{\theta\theta}(90°) > 0$ the magnetization is stable in the plane of the layer.

If Q>1, $E_{\theta\theta}(90°) > 0$ if $Hd(1 - Q) < Ha$ -> $\theta = 90°$ is a stable state only if the in-plane compensates the out-of-plane anisotropy.

Case 2:

For $\sin\theta = \frac{-H_a}{(H_d - H_u)} \rightarrow E_{\theta\theta} = -MsHd(1 - Q)(1 + 2.\frac{{H_a}^2}{(H_d - H_u)^2}) - \frac{Ms.{H_a}^2}{(H_d - H_u)}$

If Q<1, $E_{\theta\theta} < 0$ if $(H_a)^2 < (H_d - H_u)^2$ -> Not a stable point

If Q>1, $E_{\theta\theta} > 0$ if $(H_a)^2 < (H_d - H_u)^2$ -> $\sin\theta = \frac{-H_a}{(H_d - H_u)}$ is a stable point if the in-plane field does not compensate the out-of-plane anisotropy.

2. Theory of Ferromagnetic Resonance (FMR)

The theory of ferromagnetic resonance is based upon the Landau–Lifshitz–Gilbert equations, also known as LLG equations [5]:

$$\frac{d\boldsymbol{M}}{dt} = -\gamma(\boldsymbol{M}x\boldsymbol{H}_{eff}) + \frac{\alpha}{M_s}\left(\boldsymbol{M}x\frac{d\boldsymbol{M}}{dt}\right) - \gamma\frac{a_j}{M_s}(\boldsymbol{M}x(\boldsymbol{M}x\boldsymbol{P})) - \gamma b_j(\boldsymbol{M}x\boldsymbol{P})$$

Precession Damping Damping-like STT Field-like STT

The precession term dictates the oscillation of the system. The damping term corresponds to the damping "force" applied to the magnetization that oscillates.
The damping-like STT and the field-like STT correspond to the contribution of the polarized current P that can act either as a precession enhancer or a dampener of the precession.
This equation is linearized in the following system (figure 7):

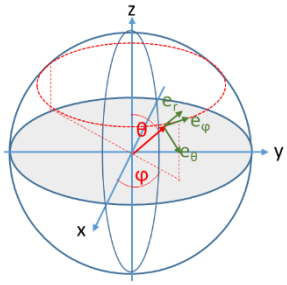

Figure 7: Schematics of the magnetization in circular coordinates system

Considering only the precession term:

$$\left(\frac{\omega_o}{\gamma}\right)^2 = \frac{E_{\theta\theta}E_{\varphi\varphi} - E_{\varphi\theta}^2}{M_s^2 sin^2\theta}$$

Considering both precession and damping term:

$$\left(\frac{\omega}{\gamma'}\right) = \frac{i}{2}\frac{\Delta\omega_o}{\gamma} \pm \sqrt{-\frac{1}{4}\left(\frac{\Delta\omega_o}{\gamma}\right)^2 + (1+\alpha^2)\left(\frac{\omega_o}{\gamma}\right)^2}$$

With:

$\left(\frac{\omega_o}{\gamma}\right)^2 = \frac{E_{\theta\theta}E_{\varphi\varphi} - E_{\varphi\theta}^2}{M_s^2 sin^2\theta}$, $\frac{\Delta\omega_o}{\gamma} = \alpha\left(\frac{E_{\varphi\varphi}}{M_s sin^2\theta} + \frac{E_{\theta\theta}}{M_s}\right)$ the linewidth.

Considering the precession term, the damping and the STT:

$$\left(\frac{\omega}{\gamma'}\right) = \frac{i}{2}\left[\frac{\Delta\omega o}{\gamma} + 2\alpha b_j P_r + 2a_j P_r\right] \pm \sqrt{-\frac{1}{4}\left[\frac{\Delta\omega o}{\gamma} + 2\alpha b_j P_r + 2a_j P_r\right]^2 + (1+\alpha^2)\left[\left(\frac{\omega_o}{\gamma}\right)^2 + \left(b_j P_r\right)^2 + b_j P_r\left(\frac{E_{\varphi\varphi}}{M_s sin^2\theta} + \frac{E_{\theta\theta}}{M_s}\right) + \left(a_j P_r\right)^2\right]}$$

C. Spin Tranfer Torque

1. Operation principle

The GMR and TMR sees the magnetization of the layers affect the current flowing through the junction. The Spin Transfer Torque, or STT, is the reciprocal effect: the current, which must be high enough, affects the magnetization of the layer, as depicted in figure 8.

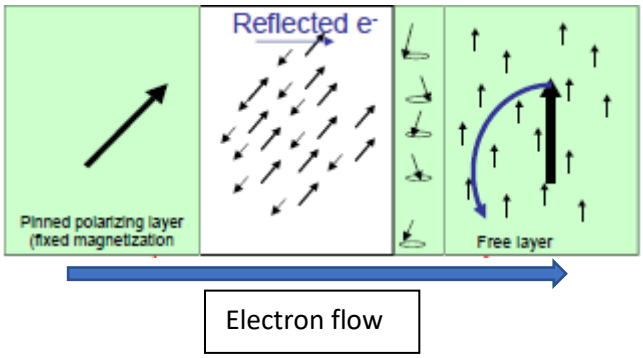

Figure 8: The STT effect in a FL/PL system.

The electrons coming from the Polarizing Layer are spin polarized, hence they can influence the magnetization of the Free Layer [6]. This principle is used to switch the magnetization in STT-MRAM and has interesting properties regarding the oscillations of magnetizations.

III. RF-to-DC conversion

When we talk about RF spintronics, there are two types of conversion possible: DC-to-RF or RF-to-DC.

A. Operation principle

The DC-to-RF conversion, also called generation, is using the oscillation of the magnetization, hence the resistance, in order to create a RF signal by injecting a DC current (figure 9).
The RF-to-DC conversion, also called rectification or detection, is using the oscillations of resistance to create a DC signal by injecting an RF current in the devices.

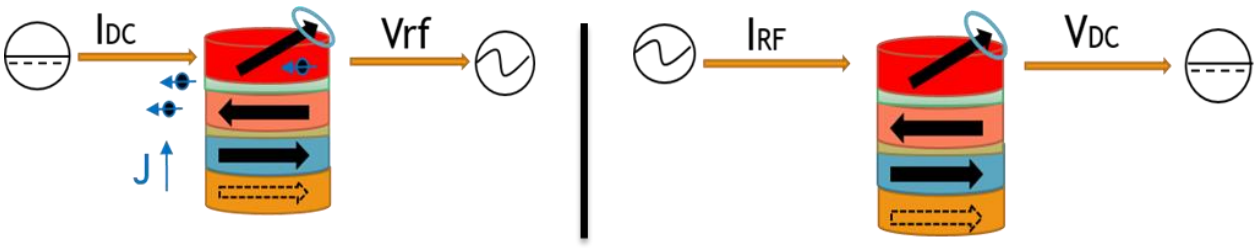

Figure 9 : On the left, DC-to-RF conversion, on the right, the RF-to-DC conversion

If we consider an oscillating resistance, R(w):

DC-to-RF conversion:

$R(w) \times Idc = V(w)$

RF-to-DC conversion:

$R(w) \times I(w) = Vdc$

If we consider:

$R(w) = R_0 cos(w_1.t)$

$I(w) = I_0 cos(w_2.t)$

$V = R(w_1) \times I(w_2)$

$$V = R_0 I_0 . cos(w_1 . t) . cos(w_2 . t) = \frac{R_0 I_0}{2} . \left[cos\left((w_1 + w_2)t\right) + cos\left((w_1 - w_2)t\right)\right]$$

With $w_1 = w_2 = w$, we have:

$$V = \frac{R_0 I_0}{2} . [cos(2wt) + 1] = Vdc + \frac{R_0 I_0}{2} . cos(2wt)$$

In this project, both principles will be used to characterize the dynamic properties of the devices. Even though we are studying the RF-to-DC conversion of a signal, a verification of the different modes through "DC-to-RF" conversion (the thermal FMR is not a DC-to-RF conversion per say, because the current applied remains below the critical current necessary to induce steady state oscillations; the DC current in the thermal FMR experiments is only necessary to convert the magnetization oscillations into a measurable signal via the TMR) might allow for a better understanding of the signals, and a better interpretation of the physical phenomena happening in those junctions.

B. Application

The main application for such devices is within a Wireless Sensor Network (WSN, figure 10), as a Wake-up receiver (WuRx), an energy harvester (WPH/WPT) or as a demodulation module (RxDemod).
The main issue of such network being the passive power consumption, especially for the reception and transmission modules. A WuRx would reduce the global power consumption by working as a secondary extremely low-power receiver used only to turn on-and-off the main transmission module whenever necessary.

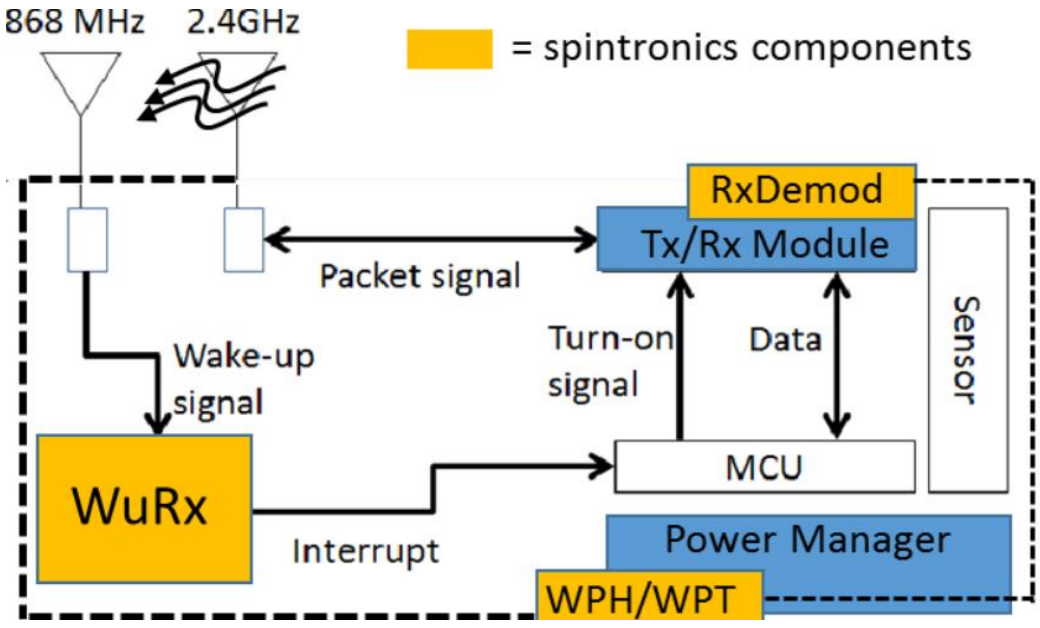

Figure 10 : A schematic of a Wireless Sensor Network with spintronics components

IV. Experimental setup

There are two types of measurements that are realized in order to understand the physical phenomena that that describes the response signal of the MTJ; MagnetoResistive Hysteresis (MRH) measurements and passive/active detection.

A. Setup for MRH measurement

Magnetoresistive Hysteresis Measurements depicts the behavior of the resistance of the junction under a sweep of an externally applied magnetic field; a DC current is applied to the junction in order to detect any variation of resistance by measuring the voltage across the junction.

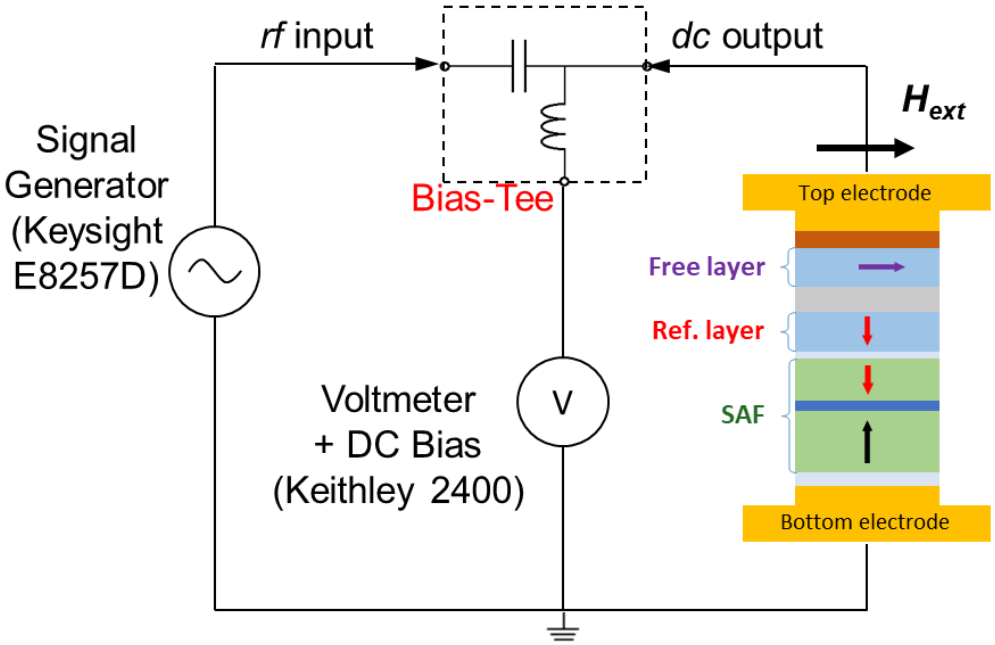

Figure 11: Experimental setup

The Bias Tee is an essential passive component in RF electronic measurements: the DC branch (connected to the inductor) only allows for a DC signal to be detected. The RF branch (connected to the capacitance) filters the DC signals that could propagate through this branch.
The sourcemeter, a Keithley 2400, provides both the DC current injected in the junction but also measures the voltage across said junction (figure 11).
An in-plane electromagnet provides the necessary field in order to observe the hysteresis effect in the device. The electromagnet is supplied by a Kepco stable source and can provide an in-plane magnetic field up to 1200 Oe.

As for the connection to the device, the probe connects the the bottom and top electrodes as such:

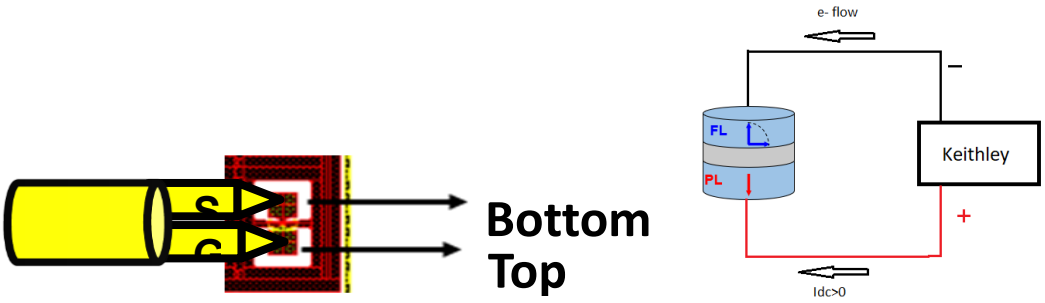

Figure 12 : The RF probe on the devices and the current in the junction

Meaning that the electron flow will travel from the Free Layer to the Polarizing Layer when the current Idc is positive (figure 12).
This information is critical since the sign of the current (along with its value) will have an influence on the device.

B. Setup for passive/ active detection

The detection (or rectification) measurement setup is similar to the MRH measurement setup, but different signals are measured : in this case, an RF current is injected in the MTJ, and the resulting rectified DC voltage is measured as a function of the frequency of the RF current.

In this setup, the RF branch of the Bias Tee prevents any DC reflected signal to be detected.
The setup is used similarly to the MRH measurement setup, but the 50-ohm load is replaced with a RF current source (Keysight).

C. Setup for Thermal FMR

The setup for thermal FMR is relatively close to the setup for DC-to-RF generation; a small DC current is injected in the junction and we observe through the spectrum analyzer the frequencies of the oscillations.

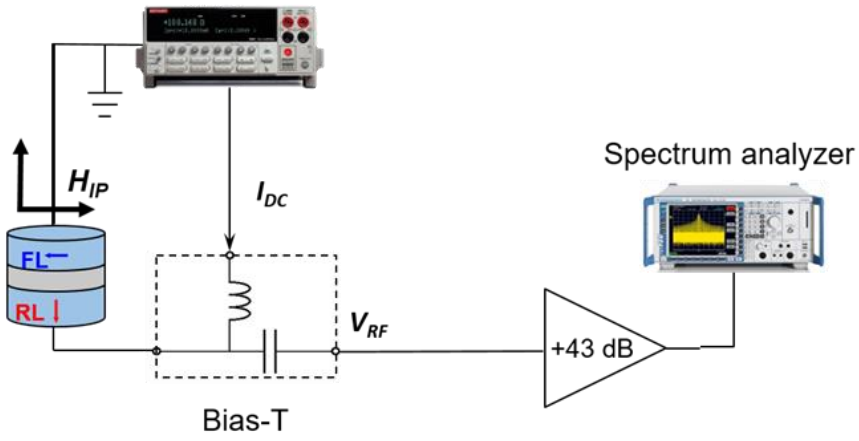

Figure 13: Experimental setup for the thermal FMR

It will be interesting to compare the detection spectra obtained with the Thermal FMR ones in order to control if the right modes are being observed, and whether the signals correspond according to the varying external parameters: current, field.

V. Experiments & Analysis

In this section, the experimental results will be described, explained and analyzed.

A. MRH

The Magnetoresistance Hysteresis measurements are an important part of the experiments since they give valuable information regarding the magnetic state of the junctions according to the diameter, the external field and the injected DC current.

As depicted on figure 14, the resistance of the junction varies according to the external in-plane magnetic field.

The stray field from the polarizer makes that in zero external field the FL is slightly tilted out of plane. When applying an in-plane field, first the FL is pulled into the film plane, going from a more parallel to a less parallel state with respect to the polarizer magnetization, thus the resistance increases. When the FL is in-plane, the rotation of the polarizer towards the in-plane direction gives rise to the decrease of the resistance, since now both magnetizations become more parallel.

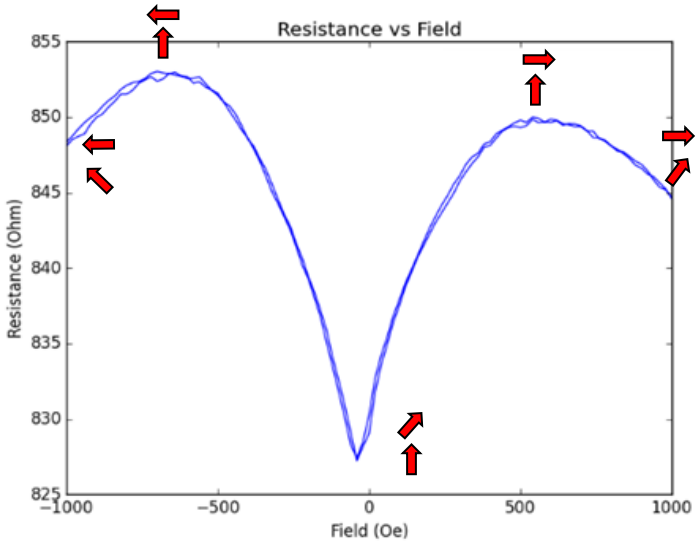

Figure 14:Typical shape of a MRH curve for t=1.6 nm

We define Q=Hu/Hd, the ratio between the anisotropy field and the demagnetizing field in the junction. The Q factor gives information regarding the compensation between the anisotropy field, $\mathrm{Hu} = \frac{2Ki}{Ms.t}$ that pulls the magnetization of the free layer out-of-plane, and the demagnetizing field Hd=$4\pi Ms.Nz$, that pulls the magnetization in-plane.

This Q factor changes with the diameter and the injected DC current.

For the 1.6 nm, the Q factor is most likely below 1, but what orients the magnetization out-of-plane is the magnetic stray field from the SAF.

This curve can be compared to the one device whose free layer thickness is 1.8nm (figure 15); as seen in II.B.1, the free layer is in-plane for this type of configuration:

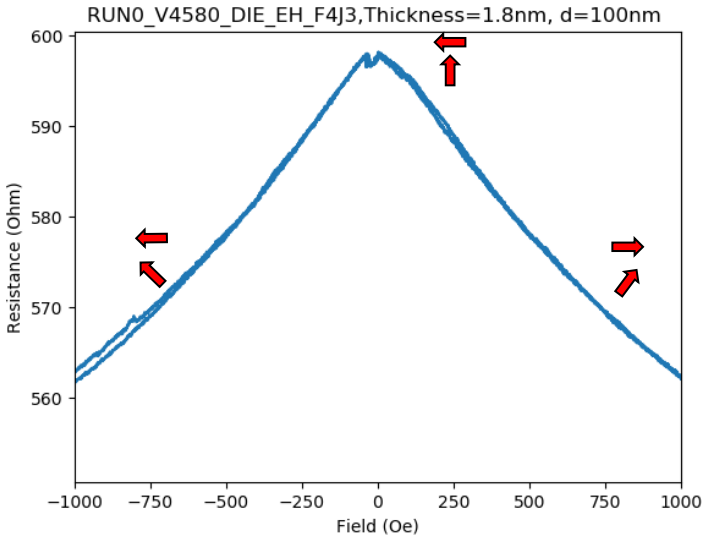

Figure 15: Typical shape of a MRH curve for t=1.8nm

For this configuration, the Q factor is always inferior to 1.

1. Diameter dependance

The diameter of the devices is a non-negligible parameter to consider.

During these experiments, we follow the resistance of the junction as a function of the applied in-plane field; we take a particular interest in the field of maximum resistance H(Rmax) to characterize the influence of the diameter on the MR curves.

The field of maximum resistance increases as the diameter decreases:

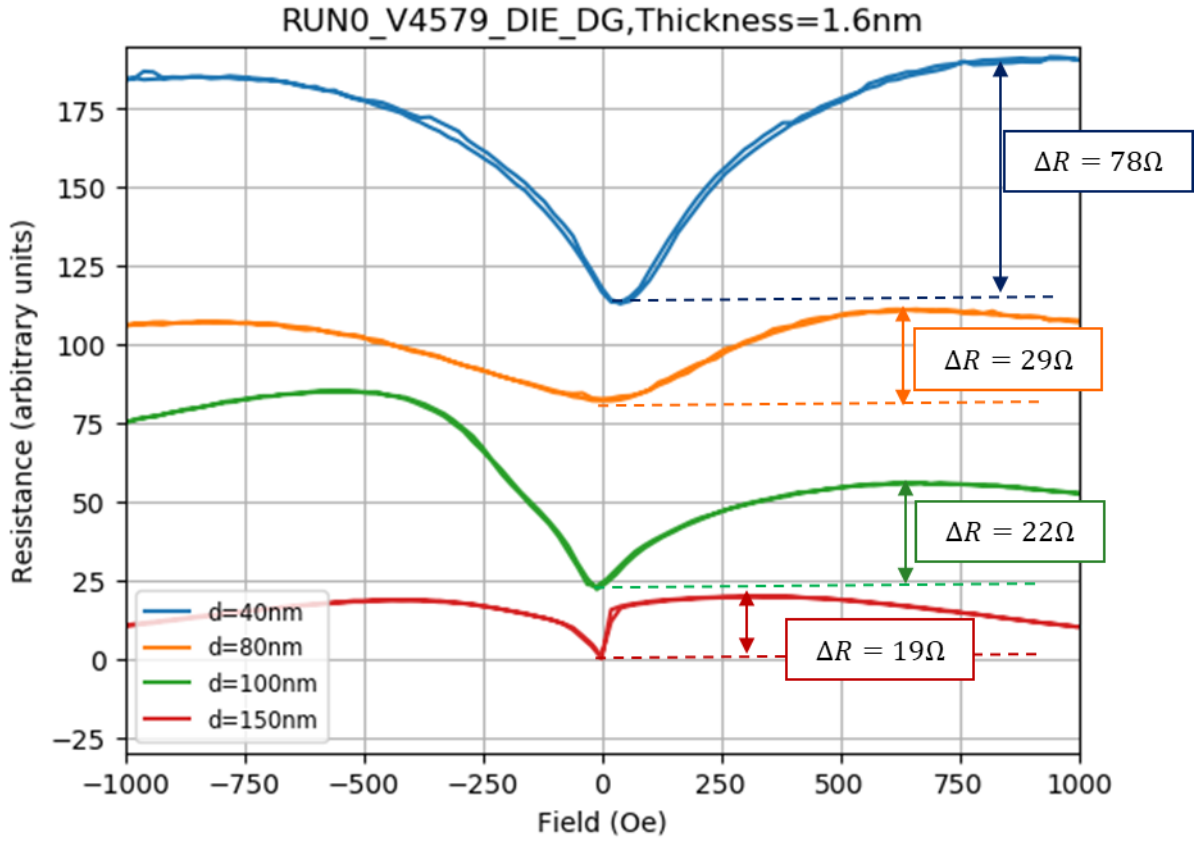

Figure 16 : MRH curve for different diameters of the junction

The resistance of each junction presented in figure 16:

150 nm	100 nm	80 nm	40 nm
400-600 Ω	700- 900 Ω	1000-1300 Ω	1800-2000 Ω

The field of maximum resistance shifts towards higher values of field as the diameter decreases:

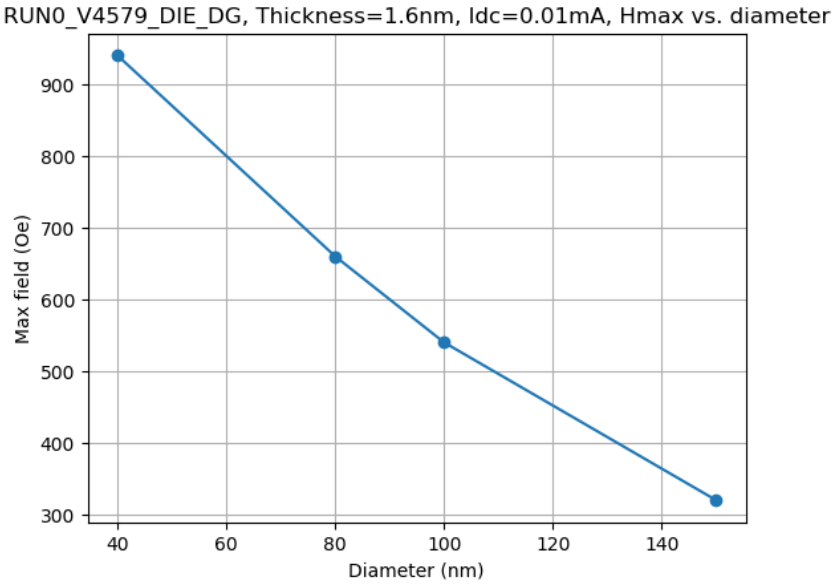

Figure 17: Field of maximum resistance as a function of diameter

The maximum of the resistance is directly linked to the saturation of the FL being aligned in-plane by the external field, i.e. the value of Hmax reflects the saturation field. The less the magnetization is tilted out-plane (in H=0), the smaller Hmax (figure 17).

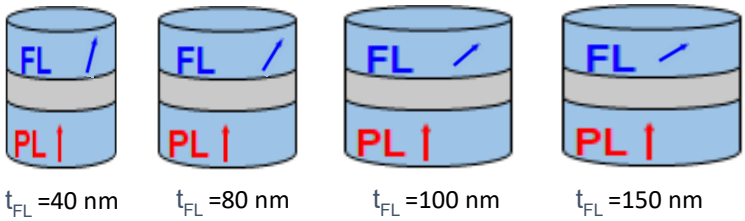

Figure 18: The four devices of different diameters

As the diameter decreases, Nz decreases, hence $Q \propto \frac{1}{Nz}$ tends to be larger, and the magnetization of the free layer is oriented out-of-plane, as detailed in figure 18.

2. Current dependance

In order to obtain the MRH curve, a DC current flowing through the junction is necessary; however, the intensity and the sign of such current will affect the magnetic states of the device.

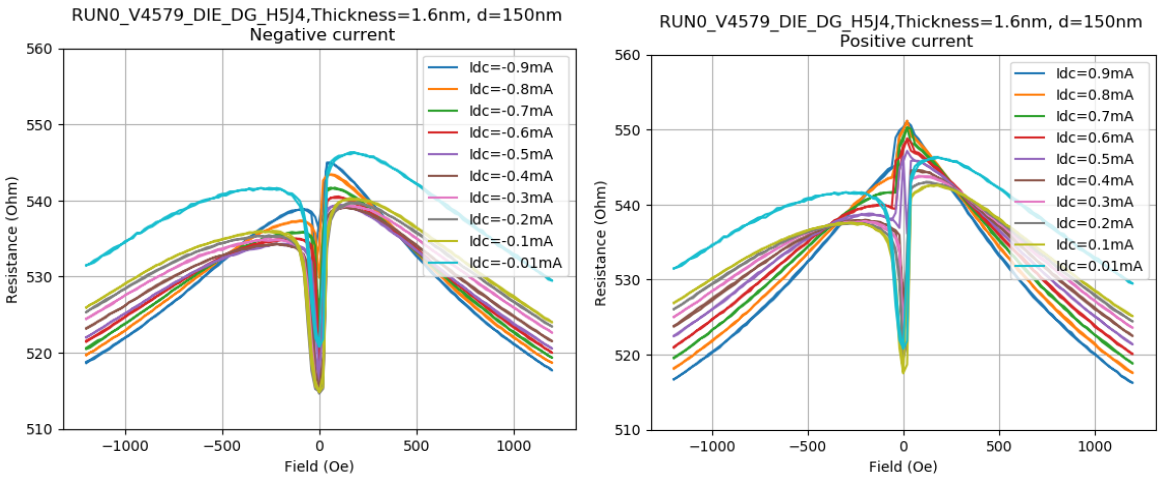

Figure 19 : MRH curves under applied DC current, on the left, for a negative current, on the right, for a positive current

At first glance, we observe a shift of the field of maximum resistance with the injected current:

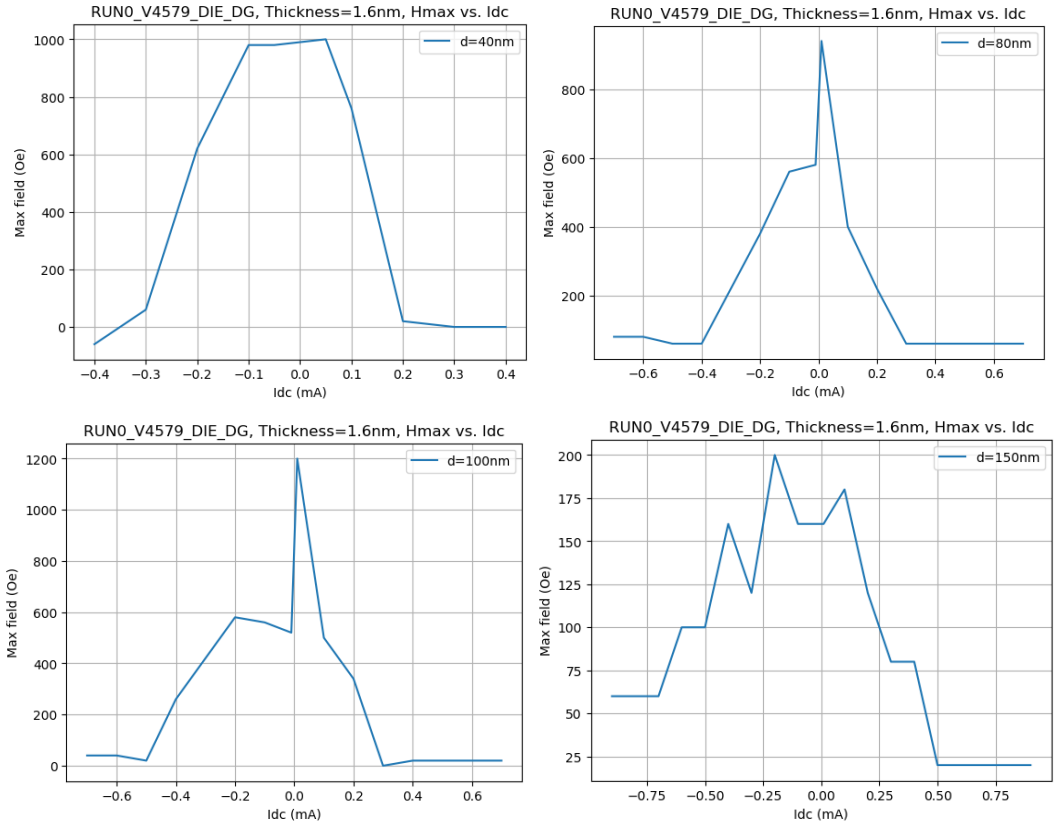

Figure 20 : The dependance of H(Rmax) with the current for 40,80,100 and 150nm diameter devices.

The quasi-symmetric curves of figure 20 hints to an effect of the current independent from its sign. An heating effect would explain such a shift in the field of maximum resistance ; the anisotropy constant

(Ku), that dictates the strength of the anisotropy field $\mathrm{Hu} = \frac{2Ki}{Ms.t}$, is affected by the temperature such as : $K_u(T) = K_0\left[1 - d\left(\frac{T}{T_C}\right)\right]\left[\frac{M_S(T)}{M_{S0}}\right]^C$, where K_0 is the anisotropy at T=0 K, Ms0 the spontaneous magnetization at T=0K, Ms the magnetization and Tc the Curie temperature, d and c being constant.
If the temperature increases, then K_u decreases, hence Ha decreases, and Q decreases. The magnetization of the free layer is oriented in-plane as the temperature (here the current) increases.

When we look closer around zero field, we can see that the contribution of the current is different according to its sign:

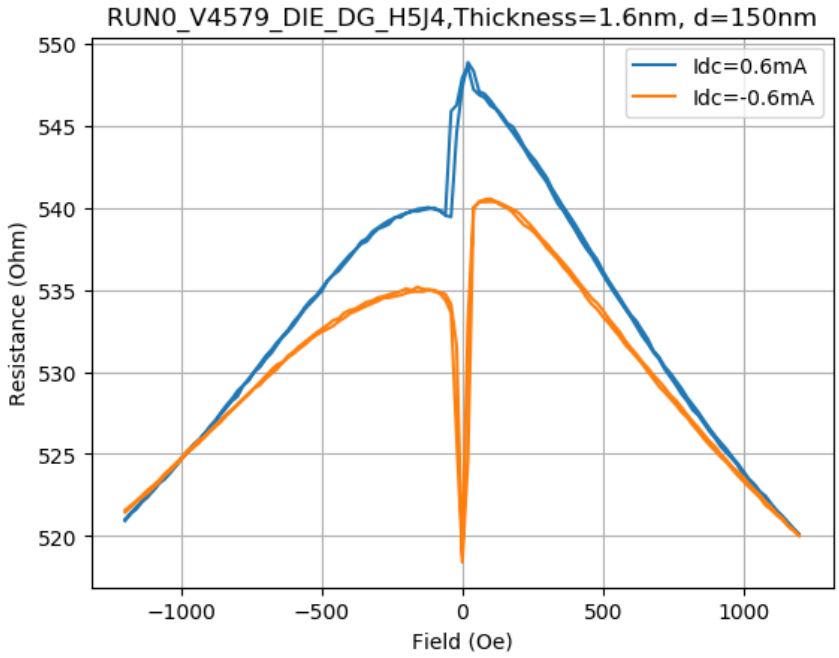

Figure 21: Comparison of negative/positive current MRH

This device (H5J4), presents a maximum of TMR of 65.13%, with Rmin=483.33ohm and Rmax=798.15ohm, hence $\Delta R = 314.81$ ohm.
For Idc=0.6mA, we observe a 9-ohm resistance variation around zero field (figure 20).
The conductivity in the junction can be defined as:

$$G(\theta) = Gp - \frac{\Delta G}{2}(1 - \cos(\theta)) \; with \; \Delta G = Gp - Gap$$

We now try to compute the angle that would correspond to the "jump" observed in the MRH around zero field; this would then give us information about the effect of a high current on the magnetization.

$$G(\theta 1) - G(\theta 2) = Gp - \frac{\Delta G}{2}(1 - \cos(\theta 1)) - Gp + \frac{\Delta G}{2}(1 - \cos(\theta 2))$$

$$= -\frac{\Delta G}{2}(1 - \cos(\theta 1)) + \frac{\Delta G}{2}(1 - \cos(\theta 2))$$

$$= \frac{\Delta G}{2}\cos(\theta 1) - \frac{\Delta G}{2}\cos(\theta 2) = \frac{\Delta G}{2}(\cos(\theta 1) - \cos(\theta 2))$$

$$= -\Delta G.\, sin\frac{\theta 1 + \theta 2}{2} sin\frac{\theta 1 - \theta 2}{2}$$

First approximation: $\theta 1 \approx \theta 2 \approx 90°$

$$G(\theta 1) - G(\theta 2) = -\Delta G.\frac{\theta 1-\theta 2}{2} \rightarrow \theta 1 - \theta 2 \approx 2.\frac{G(\theta 2)-G(\theta 1)}{\Delta G}$$=4.26°

We can deduce that the current influenced the magnetic states of the layers, changing the angle between the 2 layers, which could hint to an STT effect on the MRH curves.

B. Detection

We want to find the configurations (diameters, FL thickness) as well as external conditions (applied field in-plane, out-of-plane, current) for which the detection signal is largest. Therefore, I have studied the passive and active detection for devices of different diameters as well as for different fields. Finally, the RF power injected in the junctions was also investigated.

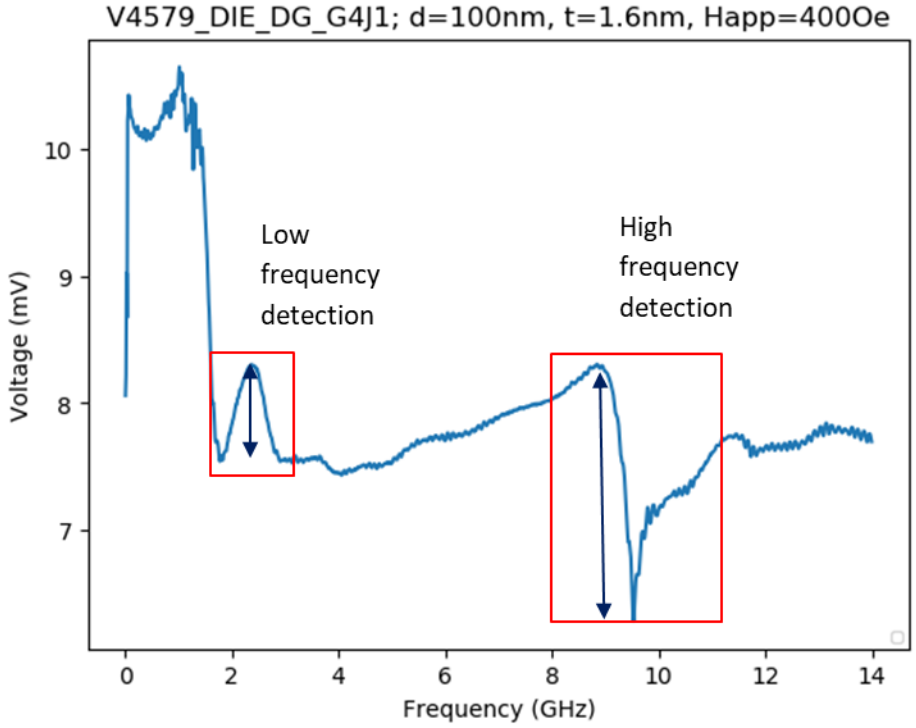

Figure 22: Typical signal of passive detection under an in-plane field

We call passive detection a measurement of detection where no current (or at most a very weak current) flows through the device.
We call active detection a measurement where a DC current is injected in the device at the same time as an RF signal.
The signal in figure 22 presents 2 modes: a low frequency and a high frequency mode.

1. In-plane field dependance – Passive detection

a) Detection spectra and FMR spectra vs. Happ

Since the external field has a critical impact on the MRH curve, hence on the magnetic states in each layer, a magnetic field will influence the oscillation of the magnetization, and on the detection.

As presented in figure 23, the field affects both frequencies, shifting them towards higher values:

We can observe that the frequency of oscillation is shifting, but also that the amplitude of oscillation (particularly for the 2nd frequency) is increasing as the field increases.

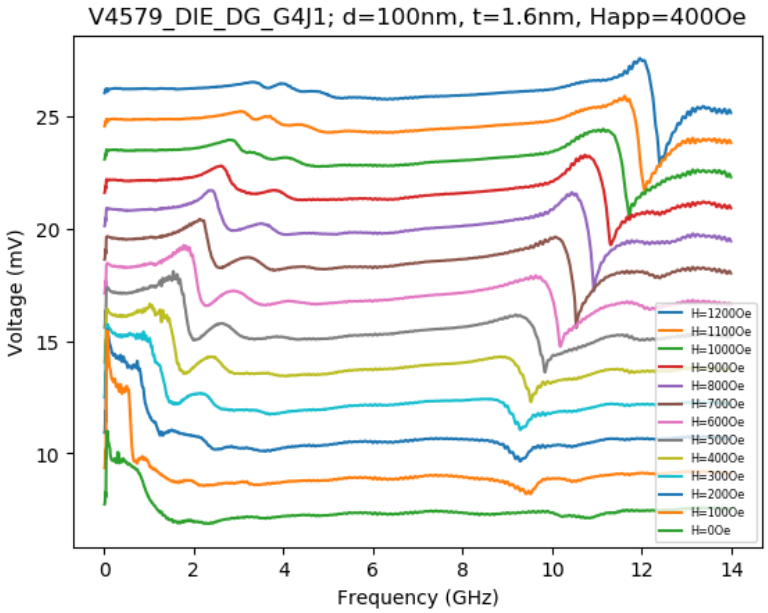

Figure 23: Effect of the external field on the detection spectra

In order to understand the shift of frequency as the field increases, we take a closer look at the thermal FMR curves for this device.
However, since the thermal FMR experiments highly depends on the injected DC current in order to visualize the resonance frequency, we need to observe them at a higher current in order to properly differentiate each peak for each field.

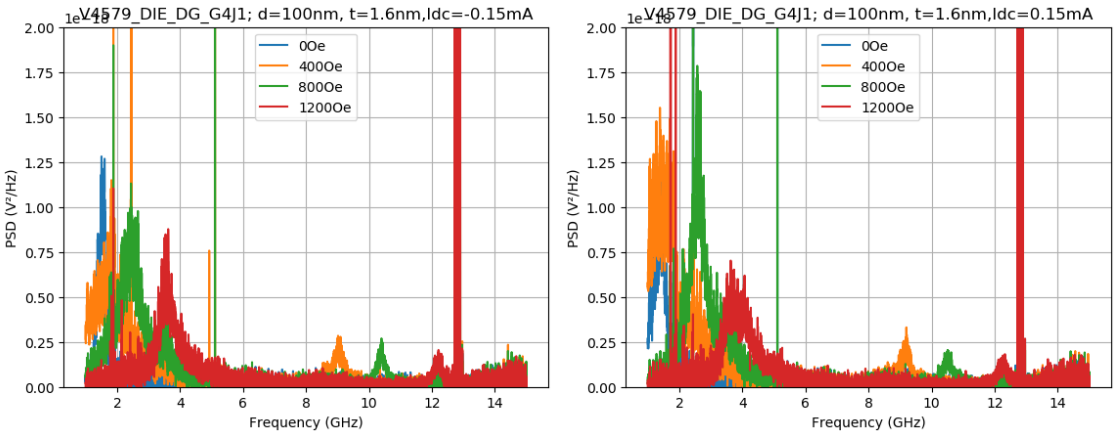

Figure 24 : FMR spectra for different field under negative (left) and positive (right) current

The figure 24 depicts the shift of frequency with the in-plane field. We can now extract the oscillation frequency and compare it to the frequency of detection that are extracted for the detection spectra (figure 25).

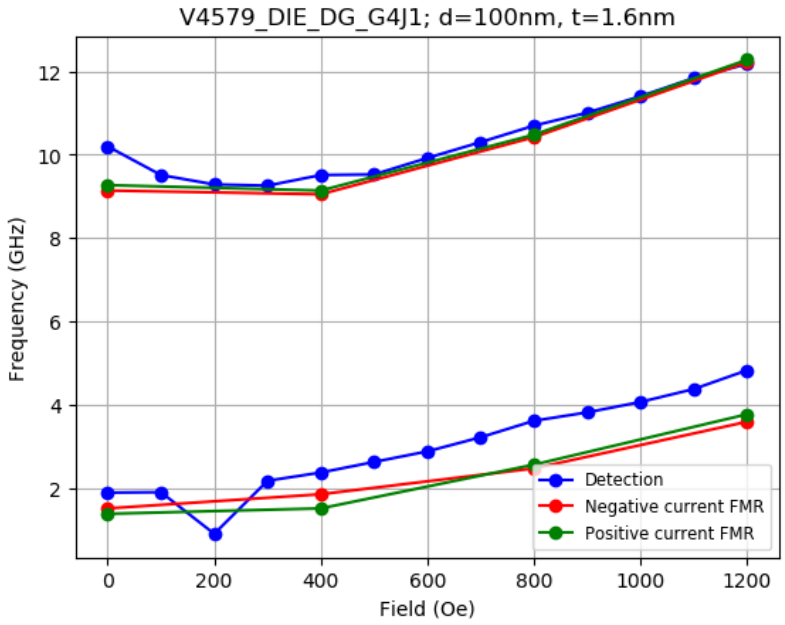

Figure 25 : Frequency shift for the detection and the thermal FMR

The high frequency detection seems to match with the thermal FMR measurements. On the other hand, a slight shift in the frequencies can be observed for the low frequency detection; this shift can be due to a more significant impact of current (or temperature) on the low frequency resonance.

The diameter being a critical factor regarding the magnetic state of the junction, we can plot the dependence between the external field and the main resonance frequencies for all diameters:

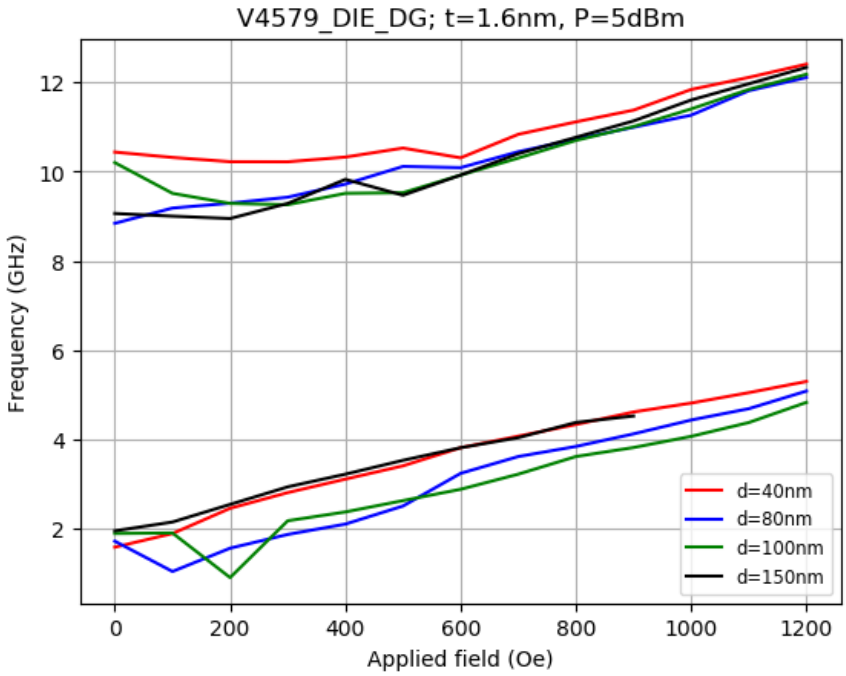

Figure 26:Shift of frequency with external field

As the field increases, the frequencies are increasing.
According to II.B.2, the frequency of oscillations under an in-plane field is:

$$\left(\frac{\omega}{\gamma}\right)^2 = H_a\left(H_a + H_d(1-Q)\right)$$

However, the diameter of the junction does not have a significant effect on the frequency shift, and the modes seem to converge for high values of field (figure 26).

b) Analysis of Vdc vs. Happ

We can now focus on the amplitude of the detection signal depending on the external field. We measure the amplitude for both frequencies for the 100nm-device.

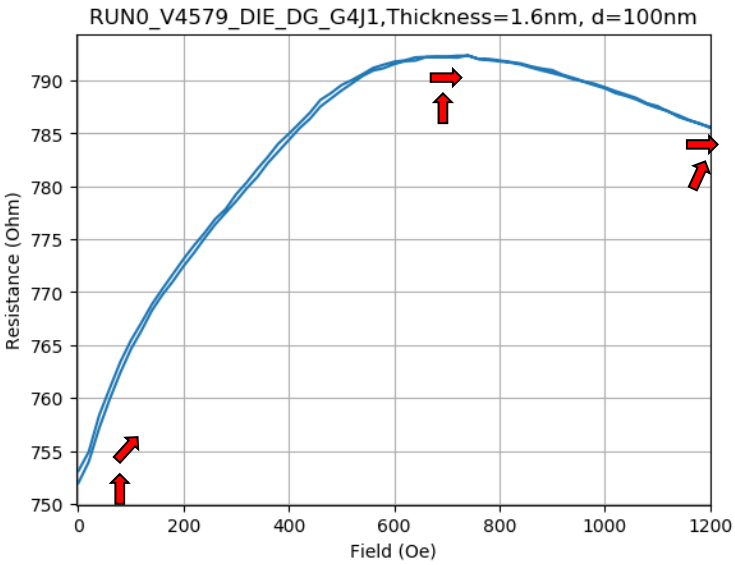

Figure 27 : MRH curve for a 100nm device (positive field only)

These plots should be put in perspective with an MRH plot, figure 26, in order to interpret the behavior of the amplitude (figure 27 and 28).

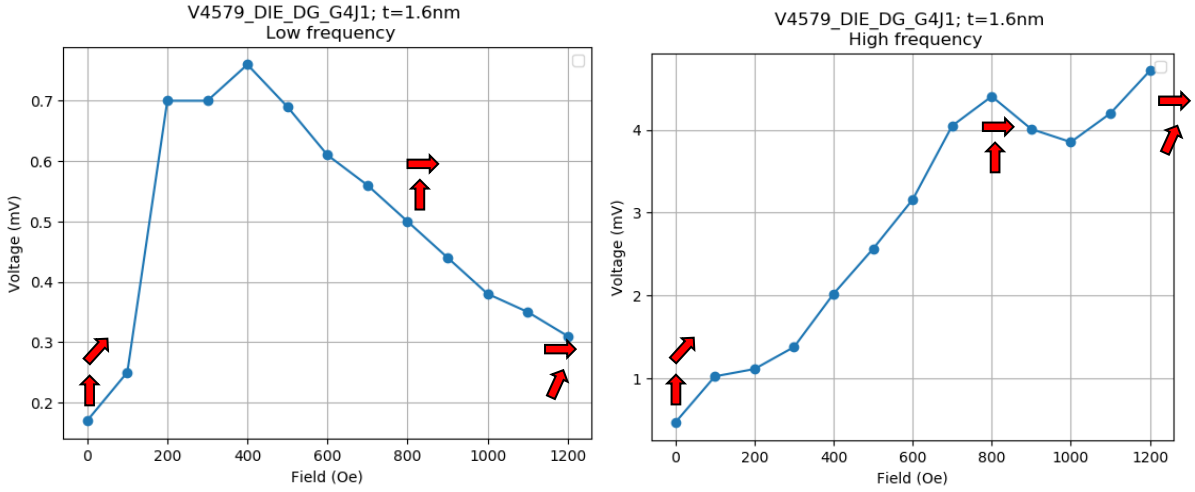

Figure 28: On the left, the amplitude of detection vs. Happ for the low frequency detection, on the right, the amplitude of detection vs. Happ for the high frequency detection

The free layer becomes more rigid as the field increases, the amplitude of oscillations hence decreases. The polarizing layer slightly tilts as the field increases; the external field compensates the internal field and makes the magnetization “softer”, meaning more susceptible to external parameters, but also makes it oscillates with larger amplitudes of oscillations.
We can now compare these amplitudes of oscillations for each diameter:

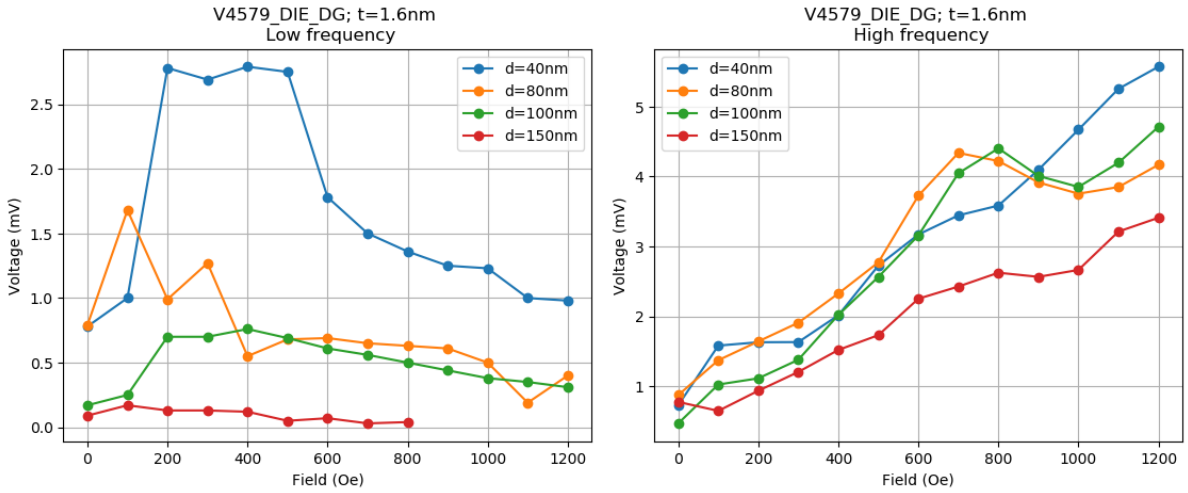

Figure 29 : On the left, the amplitude of detection vs. Happ for the low frequency detection, on the right, the amplitude of detection vs. Happ for the high frequency detection

The smaller diameter gives the best amplitude of oscillations in both cases, and the 150 nm gives a weaker signal. The 80nm and 100nm devices seem to have similar features when it comes to the amplitude. This could be due to the variability of fabrication of these devices, that could potentially explain that their diameters could be closer, and not 20 nm, making their dynamic properties similar.

c) Note on artefacts in the spectra

At low frequency, we observe a plateau in the detection profile:

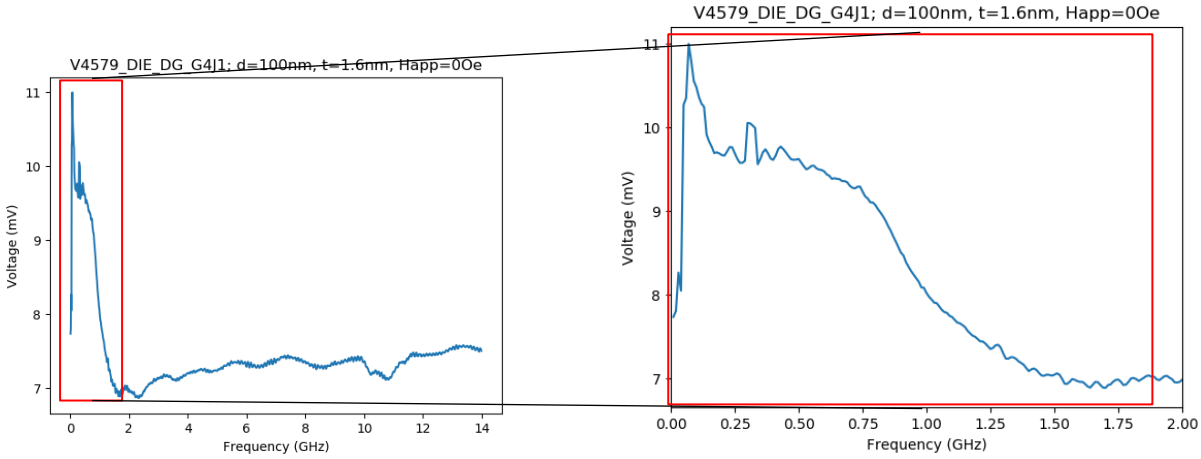

Figure 30 : Low frequency plateau under in-plane passive detection

This is a phenomenon that cannot be interpreted yet; the thermal FMR curves gives us:

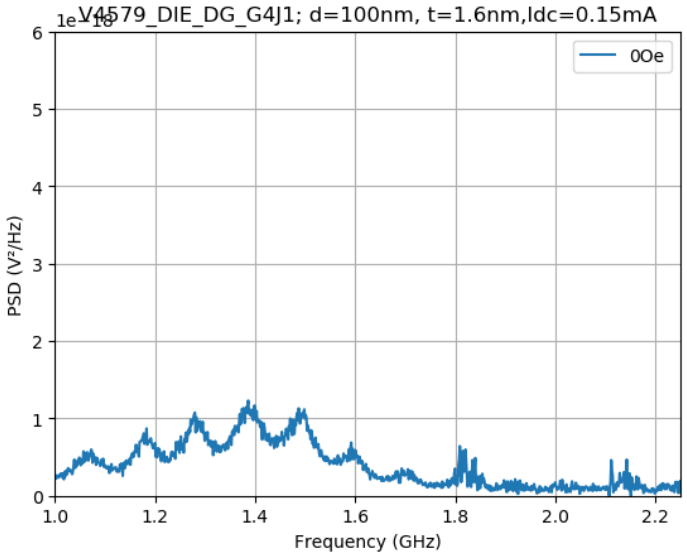

Figure 31 : Thermal FMR plot at low frequency

However, the FMR spectra does not give additional information regarding this specific low frequency signal. Figure 31 only shows a weak PSD between 1 GHz and 1.6 GHz, but the intensity of the signal does not correspond with a large detection signal.

We also observe a strong signal picked up by the Spectral analyzer around 12.81 GHz. This signal, whose linewidth is of only 1.8MHz, where the analyzer only has a 1MHz precision. Even though the signal is 3 orders of magnitudes more intense than the oscillation modes of the MTJ, we cannot explain its origin, but appears on every FMR spectra of our experiments (figure 31).

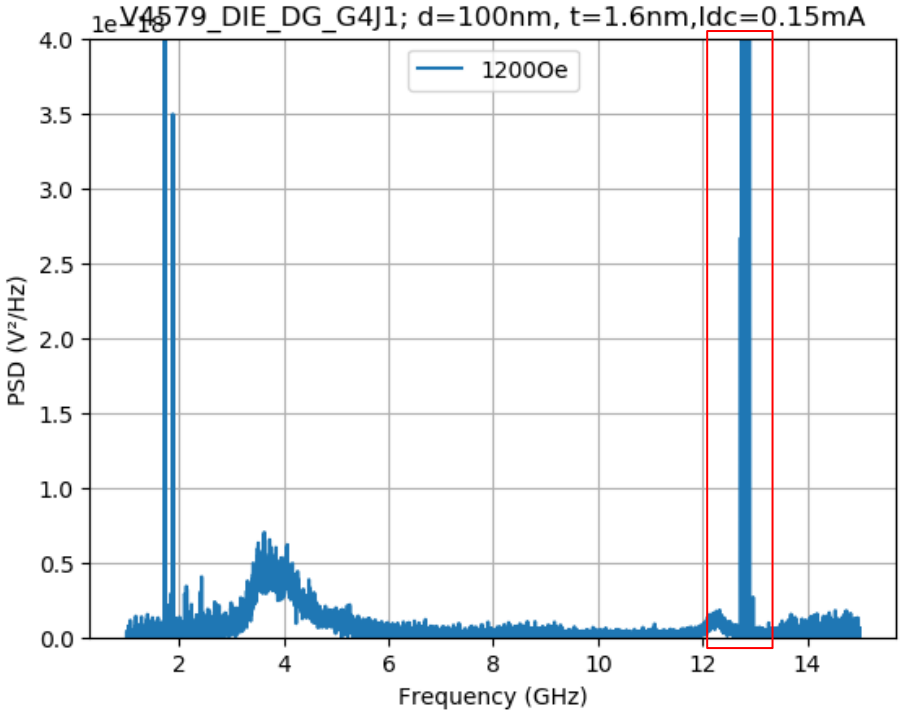

Figure 32 : Thermal FMR signal with unexplained high frequency contribution

2. Current dependance

Even though the purpose of this project is to use the devices passively (meaning with no DC current applied to minimize the power consumption), it is still interesting to observe the effect of current (and temperature).

a) In-plane field

The junction can be considered as “passive” for relatively small currents since the behavior the spectra overlay when the current is below |0.01|mA (figure 33).

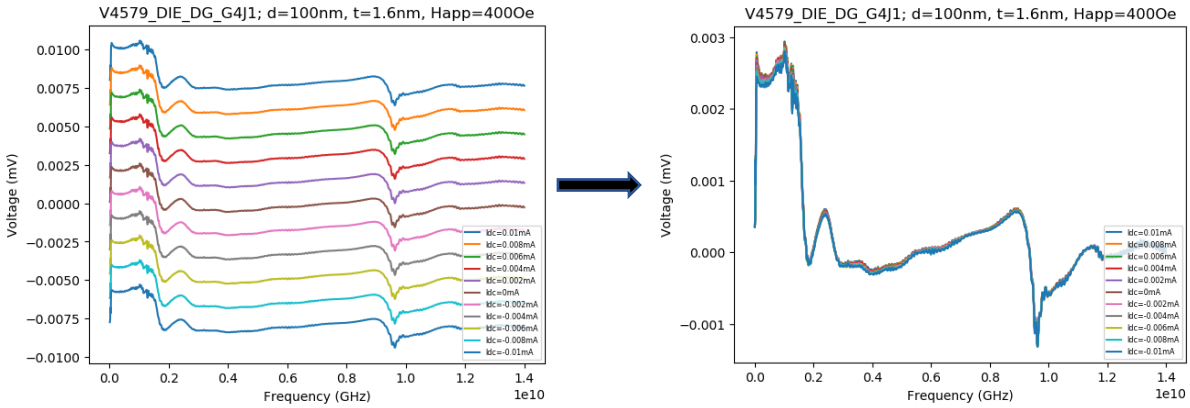

Figure 33: Effect of a small current on the detection signal

However, a stronger DC current greatly affects the detection spectra since a heating and a Spin Transfer Torque effect appear and changes the behavior of the junction.

We can now characterize the junctions of different diameters for a higher range of current.
However, in order to avoid the oxide breakdown, that would occur when the voltage across the device is ~1V, we are limited in the intensity of the current that could be injected in the device, depending on the diameter.
The figure 34 shows the dependence of the rectification signal under a DC applied current.

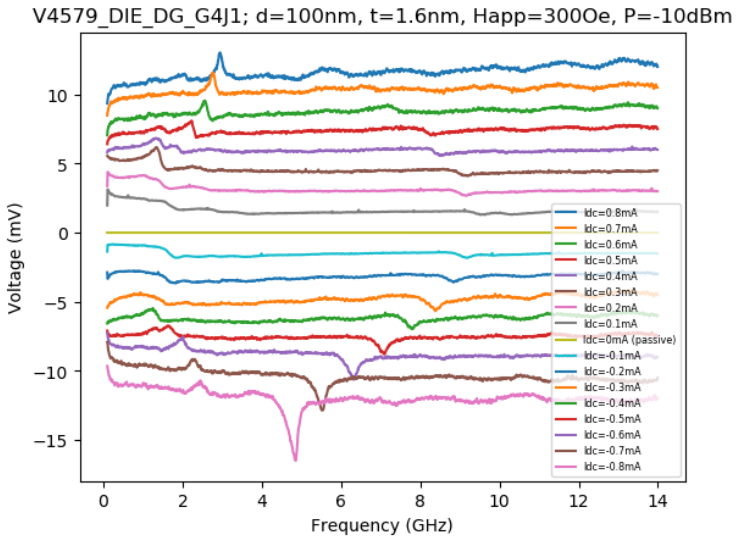

Figure 34 : Current dependence of the detection spectra

The current affects both the frequency of detection but also the amplitude of the signal.
We compare a detection signal with a thermal FMR plot in order to see if the frequency of detection match with the frequency of resonance picked up by the thermal FMR measurements.

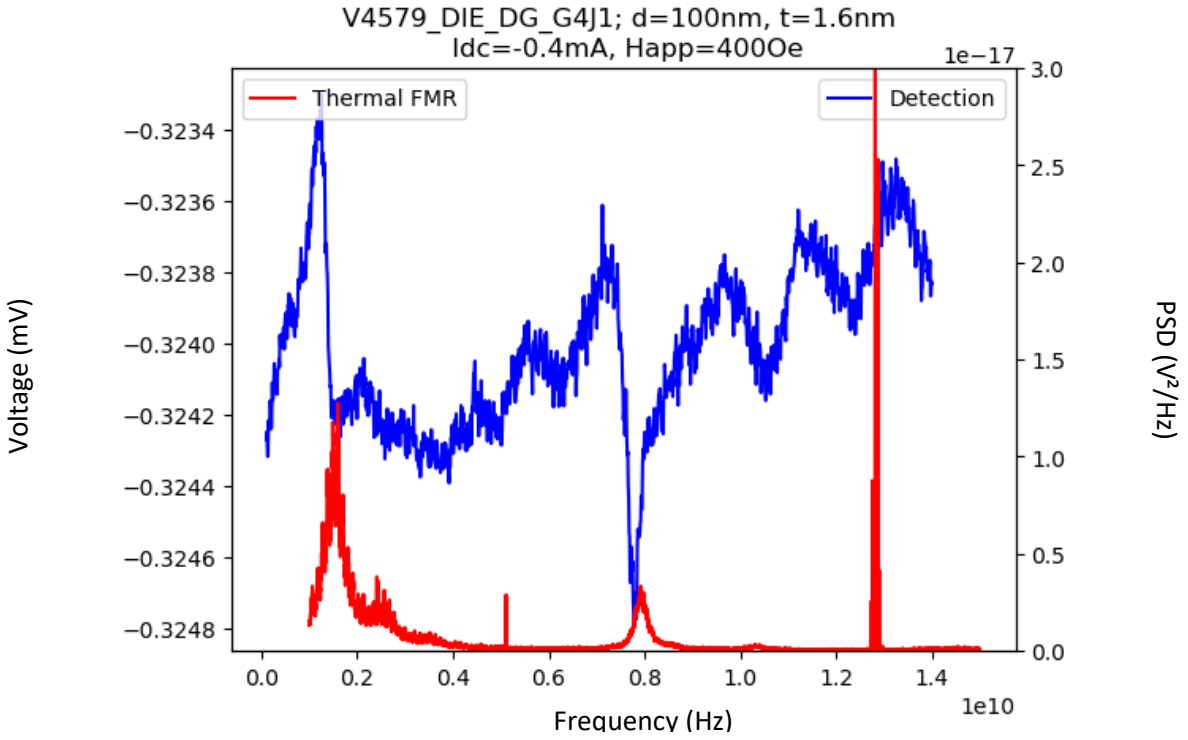

Figure 35: Correspondence between an FMR and a detection spectrum under the same field and current parameters

We can compare the dependence of the absorption frequencies with the current by comparing the shift of frequencies with the current.
Even though those two experiments are supposed to give us the same response regarding the different modes, the setup, and especially the applied field, might not be exactly the same, hence this small "shift" in the modes (Figure 35).

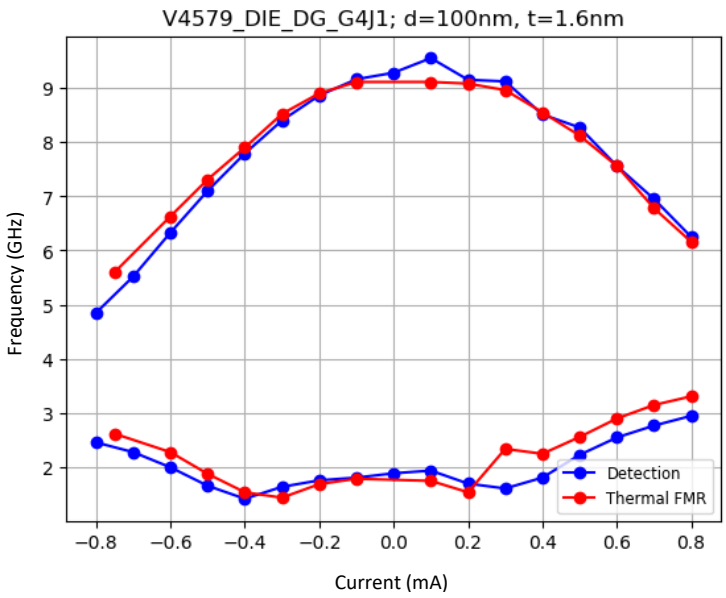

Figure 36: Shift of frequencies for Thermal FMR and detection measurements

By comparing the different modes extracted from the thermal FMR and the detection spectra, the correspondence of the frequencies seem to match in both cases as depicted in figure 35. The slight error observed could come from the fact that the setup might have changed between those two measurements and induce a slight error, especially in the applied external field.

We can take a closer look at the amplitude of the detection signal with respect to the injected current. As previously stated, the current is responsible for both a heating effect and a potential STT effect.

As seen on figure 35, the effect of current is rather symmetric on the modes of oscillations. This shift of frequency can be explained by a thermal effect of the current, especially on the Polarizing Layer, which would reduce the frequency of the oscillations. However, the amplitude of the current as an asymmetrical effect on the amplitude of the signal, as depicted by figure 37.

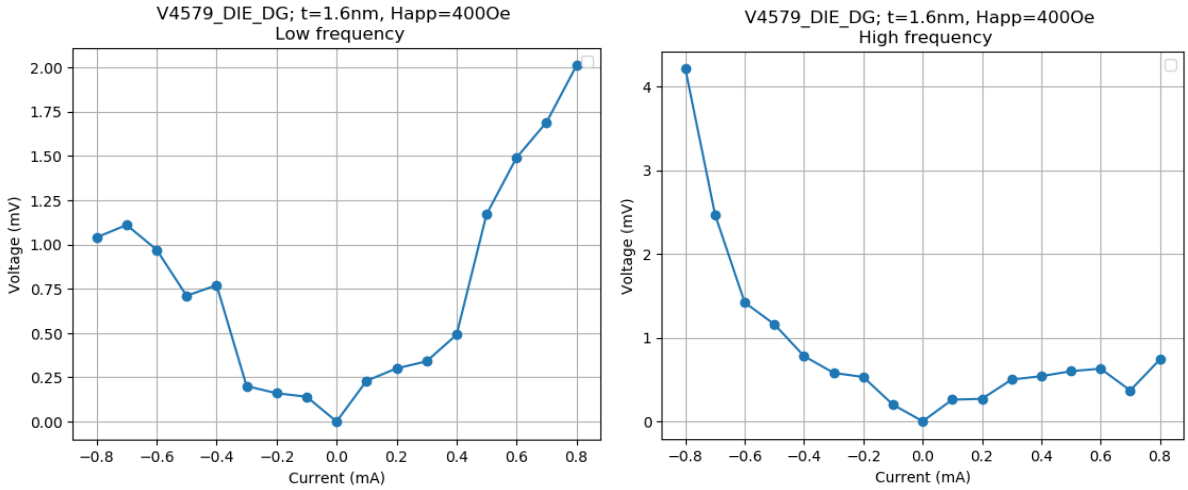

Figure 37: On the left, the amplitude of detection for the low frequency signal, on the right, the amplitude of detection for the high frequency signal

Figure 38 shows that the amplitude of the signal increases greatly for positive current for the low frequency and for negative current for the high frequency signal. The sign of the current indicates the flow of electron; a positive current means an electron flow form the FL to the PL. A negative current means an electron flow from the PL to the FL.

As seen here, a positive current enhances the oscillating properties of the low frequency (FL oscillations) whereas a negative current enhances the oscillating properties of the high frequency (PL oscillations).
This could also be verified with the thermal FMR for two asymmetric current:

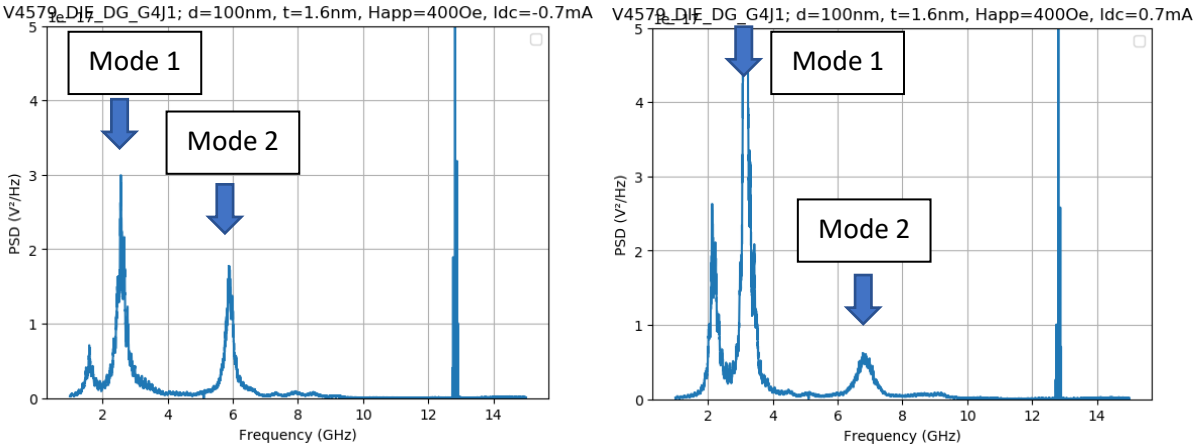

Figure 38: Thermal FMR for a negative(left) and positive (right) current

For a negative current, the oscillation around 6 GHz is increased.
For a positive current, the oscillation around 3 GHz is increased.

This enhancement of oscillations can be explained by a regime of forced oscillations, created by a strong current injected in the MTJ. The magnetization of the layers oscillates with a larger and more defined amplitude due to an STT effect, here an effective field-like effect. Hence, the detection of the signal shows a much larger amplitude than without any current injected.
The amplitude is not the only characteristic that the current affects; the linewidth of the signal gets narrower as the current increases, as depicted in figure 39.

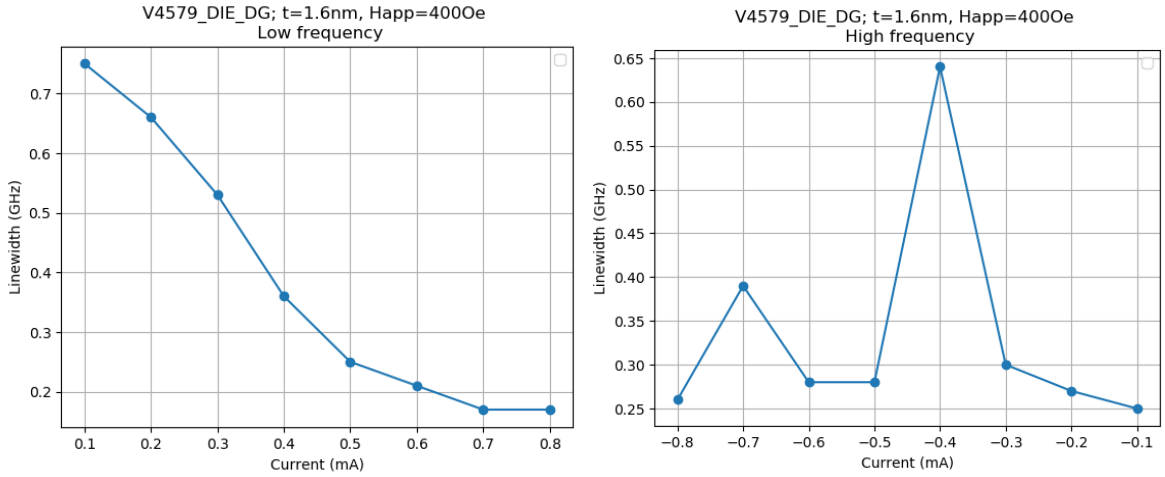

Figure 39 : Linewidth for both detection frequencies

At least for the low frequency signal, the current seems to have a significant impact on the linewidth, making the detection sharper.

b) Out-of-plane field

Since the external field has a significant impact on the magnetization dynamics, it was also interesting to study the effect of an out-of-plane external magnetic field on the devices. However, our setup could

not allow for a varying out-of-plane field to be applied, hence a permanent magnet was used to create a constant field of roughly ~1.5 to 2kOe, as depicted in figure 39.

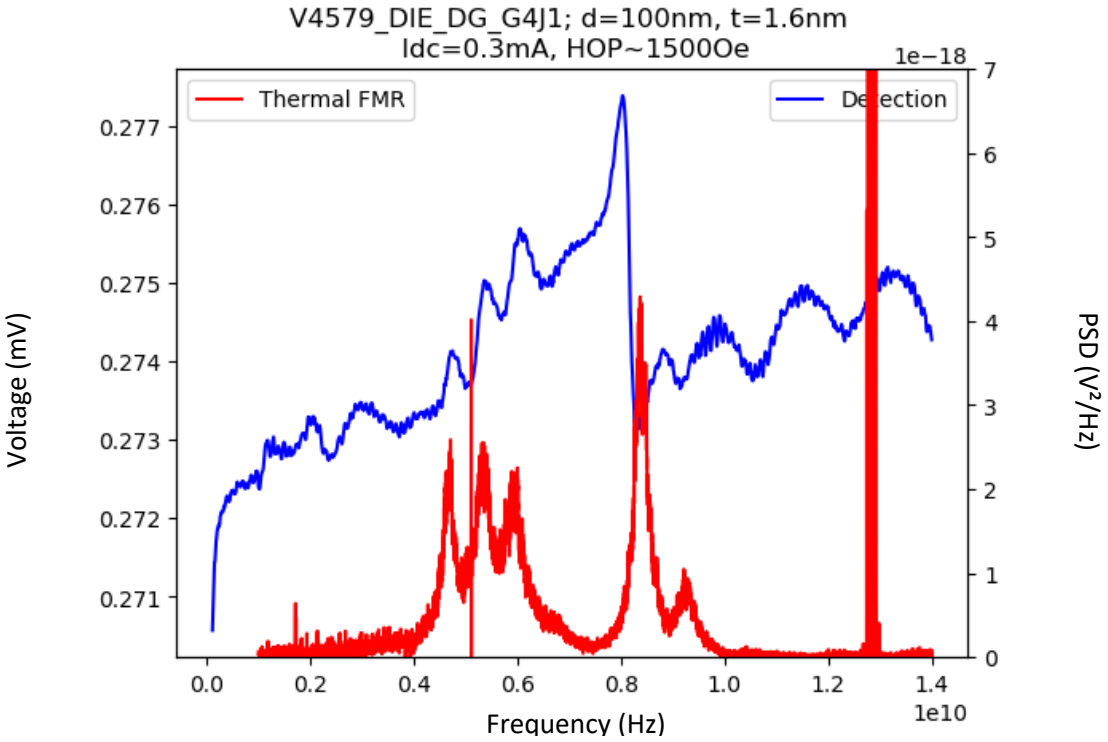

Figure 40: Correspondence of Thermal FMR and detection under an out-of-plane field

The detection signal of figure 39 shows a different shape of the signal, three modes between 4 and 6 GHz, and 2 modes around 8 and 9 GHz.
By taking a closer look at the current dependence of the junction under this configuration, we obtain the figure 41.

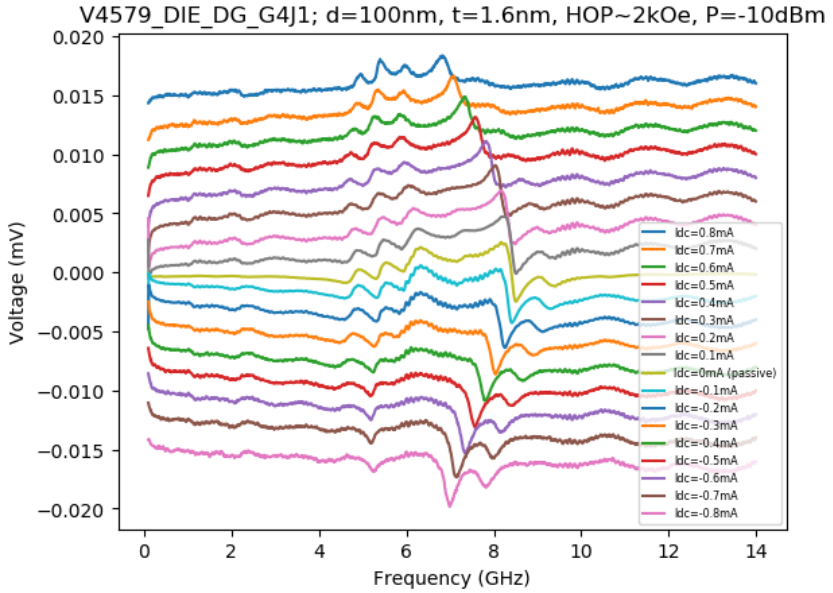

Figure 41: Current dependence of the detection under an out-of-plane field

The following figure 42 details what is considered peak 1,2,3,4 and 5.

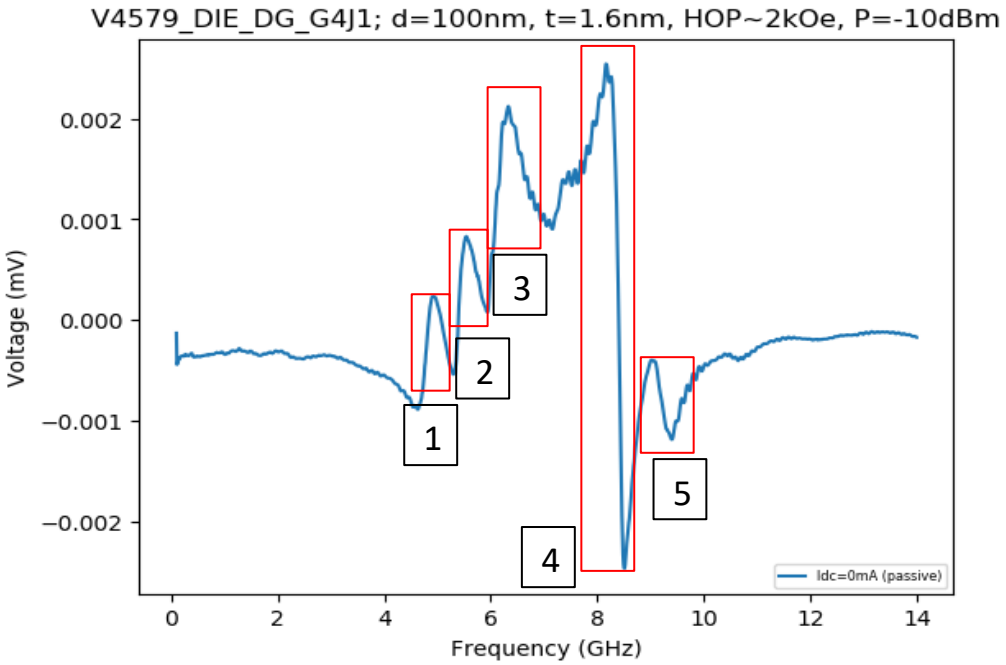

Figure 42: Detail of the detection peaks

We can now observe the shifts of frequencies with the current as depicted in figure 43.

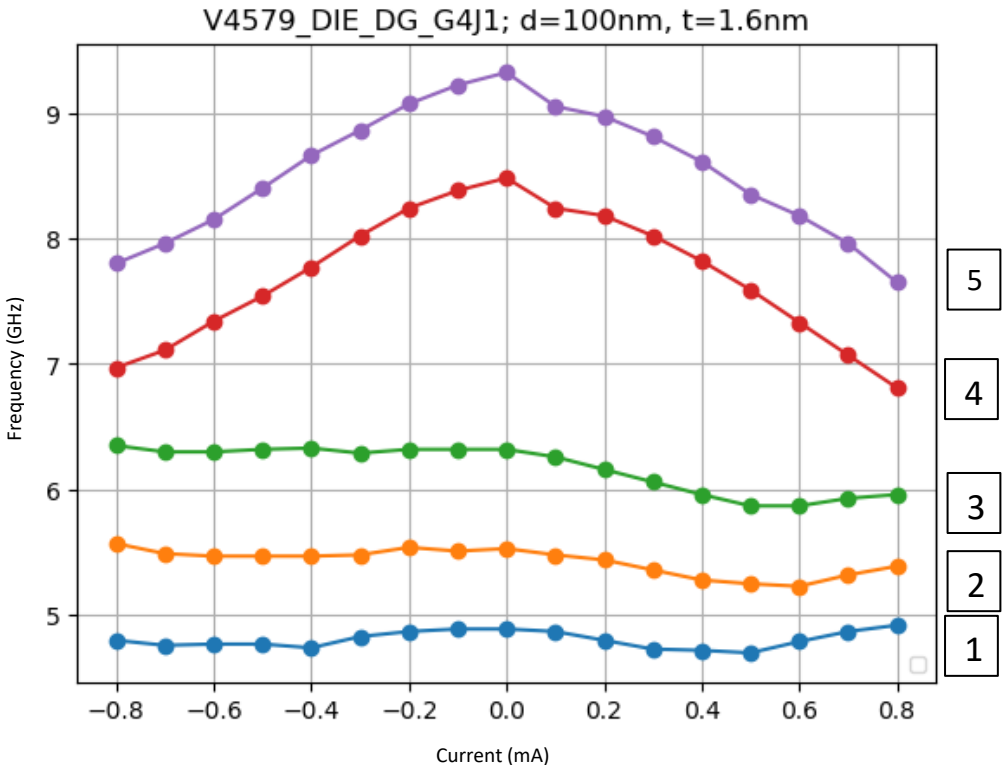

Figure 43: Shift of frequency with the current under an out-of-plane field

The shape of the curves reminds us of the previous figure 36. Only, it appears that 3 more modes are present when an out-of-plane magnetic field is applied. Given the similarities in the three modes 1, 2 and 3, we can suppose that these modes correspond to the oscillations of the FL (based on figure 36), as well as the two modes 4 and 5 could potentially indicate the oscillations of the PL.

3. Power dependance

Even though it has not been discussed before, but the efficiency and the amplitude of the conversion signal highly depends on the injected RF power.

For that, we realize the same measurements of detection on the same devices but measure the output signal for different RF power, as in figure 44.

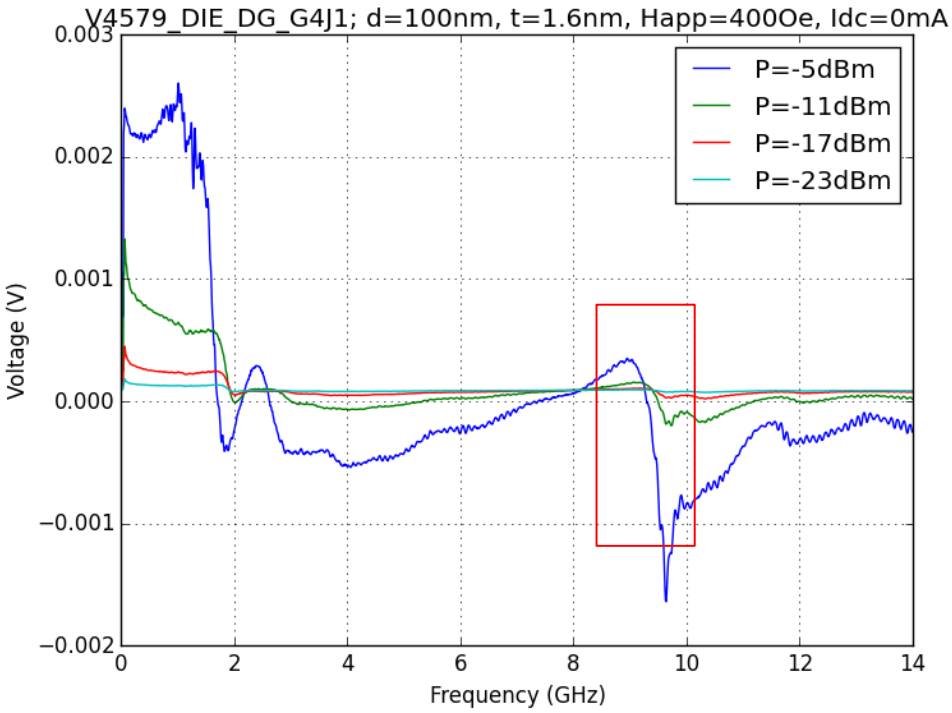

Figure 44: Details on the peaks considered for the power dependence study

We measure the amplitude as a function of the power for the high frequency detection signal, in order to compare if the diameter and the device's FL thickness influences the rectification.

a) Diameter dependence, HIP

As depicted in figure 45, the diameter does not seem to affect the amplitude of the signal when the power is reduced up to -35dBm (which correspond to 32µW).

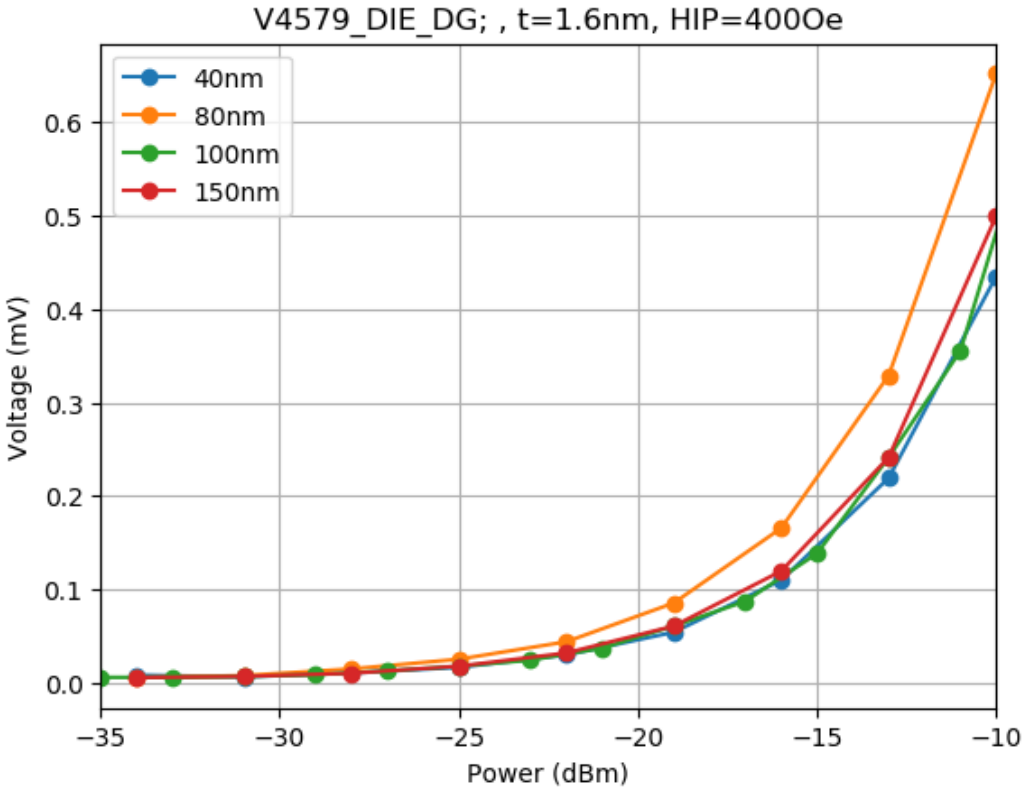

Figure 45: Comparison of the amplitudes of the signal for different diameters

However, these data were measured for all four devices with an in-plane field of 400Oe. As we saw earlier, the external field modifies the configuration of the junction, and the magnetization can be in a relatively different state.

b) Comparison with 1.4/1.8nm devices

One of the main objectives of this project is to compare the conversion efficiency of the 1.6nm devices with the 1.4nm and 1.8nm devices.
Few measurements were done on those devices but still allows us to compare with the devices measured during this project.

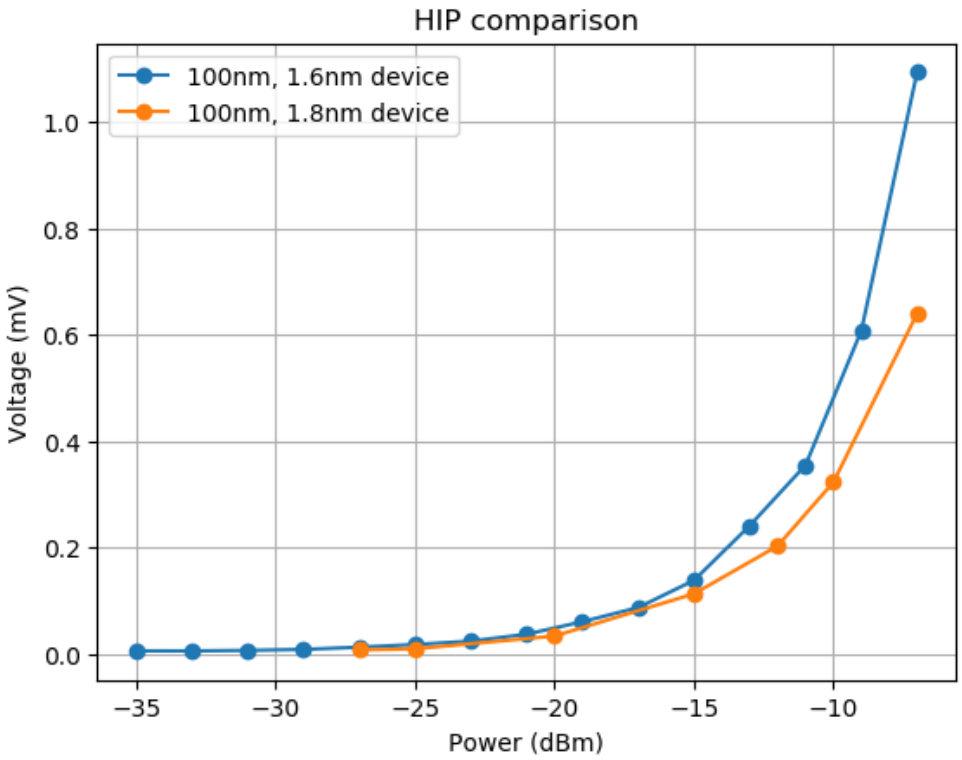

Figure 46: HIP comparison of two 100 nm devices under in-plane field of 400Oe

For a 400Oe in-plane field, only the 1.8nm and 1.6nm devices were characterized. Figure 45 shows the amplitude of the High frequency signal vary as a function of the power (dBm). The 1.6nm device shows a better RF-to-DC conversion, with a maximum difference with the 1.8nm device of ~0.4mV at -7dBm.

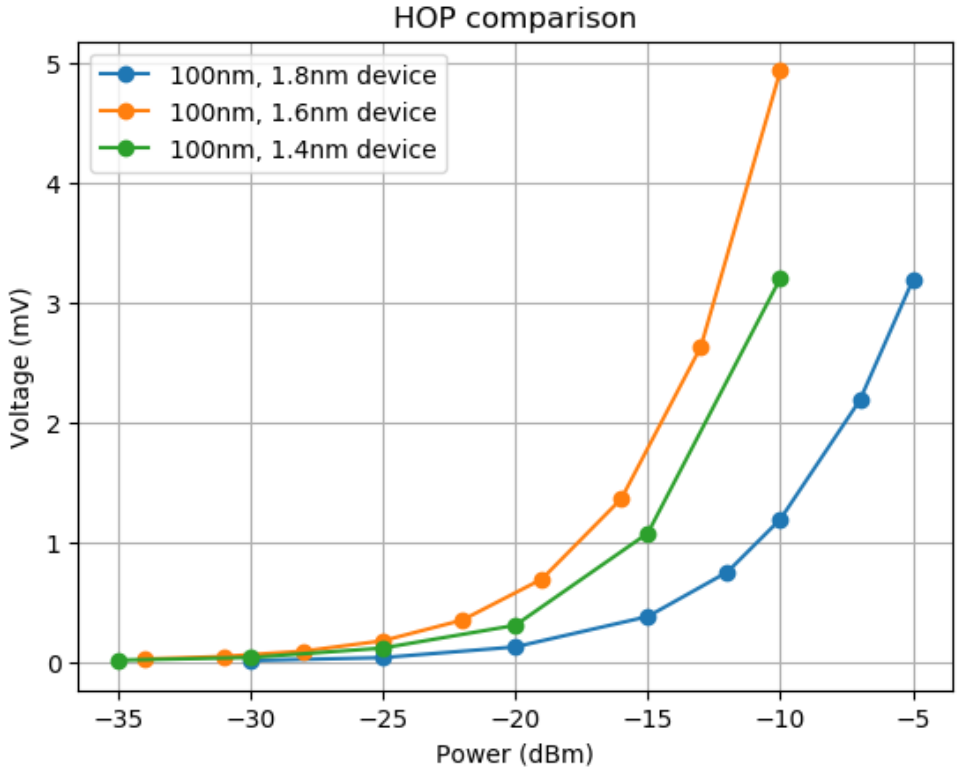

Figure 47 :HOP comparison of three 100 nm devices under in-plane field of ~2kOe

Multiple measurements were realized with a permanent magnet on all three devices (HOP~2kOe).
Once again, the 1.6nm device shows a much better RF-to-DC conversion than its 1.4nm and 1.8nm counterparts. Besides, it appears that an out-of-plane field enhances the amplitude of oscillations since the maximum of amplitude is 5 mV for a device under out-of-plane field, for 4.5 mV of maximum amplitude under a 1200Oe in-plane field for the 100nm devices.

VI. Conclusion

A. General conclusion

The purpose of this project was to understand the detection principle and to be able to characterize a device as part of a research project. In order to characterize properly those junctions, there were multiple measurements that had to be realized, to determine the static and dynamic properties of the devices according to their configuration (size, diameter) but also external parameters (external field, DC current, RF power).

The static characterization of the junctions allowed us to show that an increasing diameter of the device shifts the field of maximum resistance towards low values of field.
The same effect can be observed when a high DC current is injected in the junction; a heating effect influences the anisotropy in the junctions, making them more susceptible to an external field.

The dynamic characterization of the junction was realized both with a detection setup and a thermal FMR setup, in order to verify if the rectification modes were matching with the generation modes.
For the passive detection, an in-plane field would shift the modes towards higher values and would also increase the amplitude of the detection signal.
For the active detection, a DC current is applied to the junction. A heating effect provokes a shift of the frequencies towards lower values of frequency, while also affecting the amplitude of the signal. A positive current improves the amplitude and linewidth of the low frequency mode, while a negative current improves the high frequency mode.
An active detection study of a device was done under an out-of-plane field created by a permanent magnet. This configuration allowed us to visualize the different modes for this device, as well as the frequency shift of said modes with the current.

Finally, the devices were studied for their ability to be used for RF-to-DC conversion for low level of RF power. It would seem that the 1.6nm devices offer a larger conversion under the same external parameters, which would make them better suited for the applications of our project.

B. Personnal conclusion

Despite the exceptional circumstances in which this project was realized, it showed a lot of potential in RF applications. A further investigation on those 1.6nm devices under a varying out-of-plane field might show interesting results, with a large amplitude of detection for a low power application.
Moreover, an interesting property of stochastic switching was observed and has been repeated in a device in a particular configuration, which was the main focus of American and Japanese researcher, with potential applications in neuromorphic spintronics [7].

Bibliography

[1] Spintec - Spin in electronics Research - Grenoble - France. (2020, 15 juin). Spintec. http://www.spintec.fr/

[2] Yuasa, S. (2008). Giant Tunneling Magnetoresistance in MgO-Based Magnetic Tunnel Junctions. Journal of the Physical Society of Japan, 77(3), 031001. https://doi.org/10.1143/jpsj.77.031001

[3] M. N. Baibich, J. M. Broto, A. Fert, F. Nguyen Van Dau, and F. Petroff. (1988). Giant Magnetoresistance of (001)Fe/(001) Cr Magnetic Superlattices, Physical Review Letters.

[4] Djayaprawira, D. D., Tsunekawa, K., Nagai, M., Maehara, H., Yamagata, S., Watanabe, N., Yuasa, S., Suzuki, Y., & Ando, K. (2005). 230% room-temperature magnetoresistance in CoFeB/MgO/CoFeB magnetic tunnel junctions. Applied Physics Letters, 86(9), 092502.https://doi.org/10.1063/1.1871344

[5] Ebels, U., Houssameddine, D., Firastrau, I., Gusakova, D., Thirion, C., Dieny, B., & Buda-Prejbeanu, L. D. (2008). Macrospin description of the perpendicular polarizer-planar free-layer spin-torque oscillator. Physical Review B, 78(2), 024436-1. https://doi.org/10.1103/physrevb.78.024436

[6] Stiles, M. D., & Zangwill, A. (2002). Anatomy of spin-transfer torque. Physical Review B, 66(1), 101103. https://doi.org/10.1103/physrevb.66.014407

[7] Borders, W. A., Pervaiz, A. Z., Fukami, S., Camsari, K. Y., Ohno, H., & Datta, S. (2019). Integer factorization using stochastic magnetic tunnel junctions. Nature, 573(7774), 390-393. https://doi.org/10.1038/s41586-019-15

Abstract

This internship was carried out in the Spintec laboratory, in the Microwave devices group. The purpose of this project is to characterize the dynamic behavior Metallic Tunnel Junctions, and to demonstrate their ability to be used as RF-to-DC conversion components. A set of different devices were built for this project and were statically and dynamically characterize to observe the detection phenomenon. This project showed the dependence between the conversion and the different external parameters and junction configuration. The results show that the best RF-to-DC conversion happens for the devices with the smallest diameters, under a high in-plane or out-of-plane external magnetic field, and a high current to excite the layers.

Résumé

Ce stage a été réalisé à Spintec, dans le groupe de Dispositifs Micro-ondes. Le but de ce projet est de caractériser le comportement dynamique d'une Jonction Tunnel Magnétique, et de démontrer leur capacité de conversion d'un signal radiofréquence en signal continu. Un ensemble de dispositifs ont été fabriqué pour ce projet et ont été caractérisés statiquement et dynamiquement afin d'observer leurs propriétés de détection. Ce projet a permis de démontrer la relation entre cette conversion et les différents paramètres externes (champ, courant) ainsi que la configuration du dispositif (taille, épaisseur des couches magnétiques). Les résultats montrent que les dispositifs au plus petit diamètre présentent les meilleures amplitudes de détection, sous un champ magnétique externes fort, que ce soit dans le plan ou hors du plan, ainsi qu'un courant continu assez fort pour venir exciter dynamiquement les couches magnétiques.

Astratto

Questo stage si è svolto nel laboratorio Spintec, nel gruppo dei dispositivi a microonde. Lo scopo di questo progetto è quello di caratterizzare il comportamento dinamico dei Metallic Tunnel Junctions, e di dimostrare la loro capacità di essere utilizzati come componenti di conversione da RF a DC. Per questo progetto è stato costruito un insieme di diversi dispositivi che sono stati caratterizzati staticamente e dinamicamente per osservare il fenomeno di rilevamento. Questo progetto ha mostrato la dipendenza tra la conversione e i diversi parametri esterni e la configurazione delle giunzioni. I risultati mostrano che la migliore conversione da RF a DC avviene per i dispositivi con i diametri più piccoli, sotto un alto campo magnetico esterno in piano o fuori piano, e un'alta corrente per eccitare gli strati.